AEDC-TR-90-28

DOC_NUM   SER   CN
UNC01902-PDC   A   1

Diagnostic Measurements
on an Aluminized Propellant Plume
During Spin and Nonspin Testing
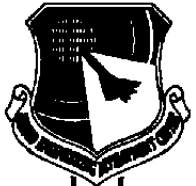
K. S. Beale et al.
Sverdrup Technology, Inc.

February 1991

Final Report for Period April through September 1990

ARNOLD ENGINEERING DEVELOPMENT CENTER
ARNOLD AIR FORCE BASE, TENNESSEE
AIR FORCE SYSTEMS COMMAND
UNITED STATES AIR FORCE

This report has been reviewed by the Office of Public Affairs (PA) and is releasable to the National Technical Information Service (NTIS). At NTIS, it will be available to the general public, including foreign nations.
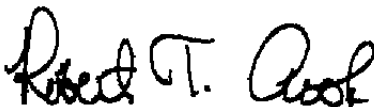
APPROVAL STATEMENT

This report has been reviewed and approved.

DAVID G. BURGESS, Capt, USAF
Facility Technology Division
Directorate of Technology
Deputy for Operations

Approved for publication:

FOR THE COMMANDER

ROBERT T. CROOK
Deputy, Director of Technology
Directorate of Technology
Deputy for Operations

REPORT DOCUMENTATION PAGE

Public reporting burden for this collection of information is estimated to average 1 hour per response, including the time for reviewing instructions, searching existing data sources, gathering and maintaining the data needed, and completing and reviewing the collection of information. Send comments regarding this burden estimate or any other aspect of this collection of information, including suggestions for reducing this burden, to Washington Headquarters Services, Directorate for Information Operations and Reports, 1215 Jefferson Davis Highway, Suite 1204, Arlington, VA 22202-4302, and to the Office of Management and Budget, Paperwork Reduction Project (0704-0188), Washington, DC 20503

1 AGENCY USE ONLY (Leave blank)	2 REPORT DATE February 1991	3 REPORT TYPE AND DATES COVERED Final Report, April to September 1990

4 TITLE AND SUBTITLE
Diagnostic Measurements on an Aluminized Propellant Plume During Spin and Nonspin Testing

5 FUNDING NUMBERS
PE - 932F01

6 AUTHOR(S)
Beale, K. S., McGregor, W. K., Frederick, R. A., Reed, R. A., and Roberds, D. W., Sverdrup Technology/AEDC Group

7 PERFORMING ORGANIZATION NAME(S) AND ADDRESS(ES)

Arnold Engineering Development Center/DOT
Air Force Systems Command
Arnold AFB, TN 37389-5000

8 PERFORMING ORGANIZATION REPORT NUMBER

AEDC-TR-90-28

9 SPONSORING/MONITORING AGENCY NAMES(S) AND ADDRESS(ES)

ARO
P. O. Box 12211
Research Triangle Park,
NC 27709-2211

NASA/MSFC
Huntsville, AL 35812

10 SPONSORING/MONITORING AGENCY REPORT NUMBER

11 SUPPLEMENTARY NOTES

Available in the Defense Technical Information Center (DTIC).

12a DISTRIBUTION/AVAILABILITY STATEMENT

Approved for public release; distribution is unlimited.

12b DISTRIBUTION CODE

13 ABSTRACT (Maximum 200 words)

Two identical aluminum-loaded solid-propellant rocket motors were tested at simulated altitudes of approximately 100,000 ft. One motor was fired under spin conditions, and the other was static-tested. Plume diagnostic measurements were made during the firings in the infrared to ultraviolet regions of the spectrum. Initial analysis of the data has been performed, and the results are summarized in this report. The data were analyzed with respect to radiant heating, searchlight emission, aluminum chloride absorption, spin effects, and particle mass distribution.

14 SUBJECT TERMS			15 NUMBER OF PAGES 53
plumes searchlight spin effects	radiant heating AlCl absorption ultraviolet	solid-propellant rocket motor infrared particle distribution	16 PRICE CODE

17 SECURITY CLASSIFICATION OF REPORT UNCLASSIFIED	18 SECURITY CLASSIFICATION OF THIS PAGE UNCLASSIFIED	19 SECURITY CLASSIFICATION OF ABSTRACT UNCLASSIFIED	20 LIMITATION OF ABSTRACT SAME AS REPORT

PREFACE

The work reported herein was conducted at the Arnold Engineering Development Center at the request of NASA and the Army Research Organization (ARO). Partial support for this work was provided by the Strategic Defense Initiative Organization (SDIO) through ARO. The results of the tests were obtained by Sverdrup Technology, Inc., AEDC Group (a Sverdrup Corporation Company), operating contractor of the propulsion test facilities, AEDC, Air Force Systems Command (AFSC), Arnold Air Force Base, Tennessee. The tests were conducted in Rocket Development Test Cell J-5 of the Engine Test Facility under Air Force Project Numbers BE08EN and DD30EW. The AEDC Air Force Program Managers for these tests were Capt. R. J. Torick, Jr., Capt. D. D. Stevens, and Capt. D. G. Burgess. The Sverdrup Project Managers were J. O. Brooks, Jr. and V. A. Zaccardi. The manuscript was submitted for publication on January 2, 1991.

CONTENTS

ILLUSTRATIONS

TABLES

1.0 INTRODUCTION

Recent diagnostic measurements on solid-propellant rocket exhaust plumes at AEDC have revealed phenomena that may assist in spectrally, spatially, and temporally characterizing plumes. These phenomena are briefly described in the following paragraphs:

- Searchlight emission is radiant energy originating within the motor that is scattered into the detector field of view (Ref. 1). This extraneous energy has recently been identified as a major contributor to near-field plume radiance in some motors. Methods of determining radiant heat transfer must be re-examined in this light.

- Measurements on aluminized motor plumes have revealed a deep ultraviolet (UV) spectral absorption feature at approximately 261 nm, which has been attributed to aluminum chloride. By applying emission/absorption techniques, absorption measurements could possibly be used for plume temperature calculations (Ref. 2).

- Some spin-tested motors have exhibited a visible "dark core" region believed to be caused by vortices induced by the spinning action of the motor. Analysis of the data has resulted in radial plots of plume radiance showing a depression in radiance level at the plume centerline that does not show up in data from static motors. The data were acquired on motors of different types, therefore shadowing the certainty that the depression was caused by spin influences.

- Radiant heating measurements from plumes have been made that do not agree well with predictions by existing heat-transfer codes. Base heating studies utilize radiation data from strategically placed heat flux transducers that could also provide information to aid in the development of a base heating model for space vehicles.

- Laser transmission measurements have been shown to be useful in determining mass and size distribution of aluminum oxide particles within aluminized propellant plumes. Past measurements have shown mass distribution within the plume to be a function of motor spin.

The opportunity was made available to apply these diagnostic measurements to two identical aluminum-loaded solid-propellant rocket motors during performance testing in AEDC Rocket Development Test Cell J-5. One motor was tested under spin conditions, and the other was static-tested. Diagnostic measurements from the mid-ultraviolet (mid-UV) to the long wavelength infrared (LWIR) were made during the motor firings to address each of the subjects described here. This report discusses initial analyses of the data from these

measurements. Further analysis of the data is expected in the future, and the results will be presented in the form of technical papers and reports at that time.

2.0 TEST DESCRIPTION

2.1 TEST ARTICLE

The solid-propellant rocket motor tested was developed to provide perigee kick performance for transferring payloads from low earth orbit to geotransfer orbit. The propellant is a standard mixture grain with ammonium perchlorate and aluminum loading. The motor is configured with a fixed nozzle assembly and has an initial nozzle expansion ratio of 80:1. An illustration of a typical solid-propellant rocket motor is presented in Fig. 1.

2.2 FACILITY

Rocket Development Test Cell J-5 (Fig. 2) is a complex for testing rocket motors horizontally at pressure altitudes up to 150,000 ft. The test chamber is 16 ft in diameter and 50 ft long and is equipped with a temperature-conditioning system designed to maintain the test cell and motor at prescribed temperatures ranging from 10 to 110°F from motor installation until prefire pumpdown. Altitude simulation is provided by a steam ejector-diffuser system in conjunction with rotating exhauster machinery. Axial and lateral forces are measured by load cells mounted on a multicomponent thrust stand. The test cell can be configured with a spin fixture capable of rotating the test motor about its axis at rates up to 100 rpm.

The spin motor discussed in this report was cantilever-mounted to the face of the Test Cell J-5 spin rig, leaving a distance of 13 in. between the motor nozzle exit plane and the test cell exhaust diffuser. The nonspin motor was mounted directly to the aft flange attachment ring with a 34-in. space between the motor and diffuser.

2.3 INSTRUMENTATION

Various instruments were installed in and around the test cell to characterize the exhaust plume with respect to temporal, spectral, and spatial radiance, radiant heat flux levels from the plume near the base of the rocket motor, and laser transmission through the plume. The measurement suite of instruments used during the tests included three infrared imaging cameras, a circular variable filter (CVF) spectrometer, a UV spectrometer, two, gated, visible cameras, four heat flux transducers or total radiometers, and a multiple-path laser transmission system. Table 1 lists all the instruments with their respective spectral range, field-of-view size, and field-of-view location relative to the motor nozzle exit. Instrument fields of view in relation to the nozzle exit and test cell diffuser are shown in Fig. 3.

2.4 CALIBRATION

Standard procedures applicable for each type instrument were used during pretest calibrations. All radiance calibrations used sources traceable to the National Institute of Standards and Technology (NIST). The IR instruments, including the IR cameras and the CVF spectrometer, were calibrated using a high-temperature blackbody. The UV spectrometer was calibrated using a diffuse reflector illuminated by deuterium and tungsten-halogen lamps. Calibration of the gated, visible cameras was not required for these tests. Factory calibrations for the heat flux transducers were verified using an NIST-traceable blackbody. The laser transmission measurements were self-calibrating during the test with the clear path signal level prior to motor ignition defining the 100-percent transmission level and a fully blocked beam defining full attenuation.

2.5 TEST PROCEDURES

Prior to firing, the spin motor was temperature-conditioned to 35 ± 5°F and the nonspin motor to 95 ± 5°F. Each test was performed with an automated countdown sequencer that coordinated operations of the test facility and data acquisition systems with operations of the motor and ignition systems. The diagnostic instruments and data systems were energized at either t − 1 min, t − 20 sec, or t − 10 sec. All diagnostic systems were turned off at t + 5 min. Both motors were tested at approximately 100,000 ft simulated altitude. Burn time for each motor was approximately 120 sec. During the spin test, the motor was rotated at a constant 35 rpm and was allowed to self-extinguish. The nonspin motor was water quenched at t + 175 sec.

2.6 MOTOR PERFORMANCE

Performance characteristics during both motor firings are presented in Table 2. Plots of measured axial thrust, chamber pressure, and test cell pressure during the burn for both tests are shown in Fig. 4.

3.0 RESULTS AND DISCUSSION

Each of the measured plume characteristics will be used, where applicable, to analyze the plume with respect to the presence of searchlight emission, the identification of aluminum chloride absorption for use in plume temperature calculations, spin effects, heat-transfer calculations, and aluminum oxide mass distribution in the external plume flow field. Further background information on each of these subjects, as well as results from these tests, follows.

3.1 HEAT-TRANSFER DETERMINATION

3.1.1 Background

The thermal load caused by plume radiation must be known to ensure adequate thermal protection for the motor base and sensitive spacecraft structures. The heat load on the space shuttle external fuel tank and other aft surfaces, for example, is primarily caused by plume radiation (Ref. 3). The NAVSTAR Global Positioning Satellite apogee kick motor similarly places a stressing radiative heat load on the solar cells and some of the aft antennas. The *a priori* prediction accuracy of plume radiative heating loads is currently inadequate for spacecraft design. As a result, plume radiative heating predictions are almost always based upon semi-empirical methods. The most widely used method is the view-factor method, sometimes called the Bobco method (Refs. 4 and 5). The principal advantages of this method are simplicity and the use of measured plume radiance. Basically, the view-factor method attempts to replace the plume by an equivalent hard body with a surface defined by the plume boundary and with a spatial radiance distribution chosen to reproduce the measured plume radiance. The plume surface is broken up into facets, and the heat load onto a target location is calculated by numerical integration over the surface. For high-altitude vacuum plumes, a simple conical plume is used. For low-altitude applications, more complicated combinations of stacked cylinders and conical sections are common. Since the plume is actually a diffuse aerosol, the use of an equivalent hard body surface is not strictly correct. Although this is probably not a major concern for a large motor like the space shuttle solid-propellant rocket booster, it becomes more important for motors in the orbital transfer size class such as the subject motors of this report. These smaller motors become optically thin emitters (i.e. volume emitters rather than surface emitters) within one or two nozzle diameters downstream of the exit plane. Even though the physics of the view-factor method is questionable for these smaller motors, it is clear that it can still be used as long as one is clever enough in the definition of the equivalent hard body emitter. This is not as simple as it sounds, however, and the failure to properly specify the correct equivalent emitter is the potential source of several systematic errors in the view-factor approach.

3.1.2 Application and Results

Heat-transfer analysis on the data from these tests has not yet been performed; however, an explanation of the method to be applied and the anticipated results are included here. The expected results are based on analyses from similar motor firings.

It is generally not possible to directly measure the parameters needed to determine the correct equivalent hard body emitter. The traditional suite of measurements employed are narrow field-of-view radiometers viewing the plume centerline at right angles to the thrust axis. The

preferred viewing orientation, of course, is not at right angles but looking along the plume axis from a location on the motor body. This is not possible in an altitude test cell, however, because the downstream diffuser is an intense source of radiation and would lead to artificially elevated radiance readings. One broadside radiometer is usually located near the exit plane and one or more at a downstream location to obtain the axial decay rate. Since the plume is not a hard body surface, the radiance at right angles is generally not the same as the small aspect angle radiance directed back toward the spacecraft. At right angles, the properties along the line of sight through the plume are fairly isothermal. For small aspect angles, on the other hand, the density and temperature vary considerably along the line of sight. The relation of the small aspect angle radiance to the measured broadside values is somewhat problematical, and one therefore has an angular extrapolation problem. The aspect angle dependence of the radiance from the subject motor, for example, is rather pronounced as shown by the low heat flux level measured by the downstream viewing total radiometer as opposed to the high levels measured by the side-on radiometers (Fig. 5). The broadside radiance close to the nozzle, moreover, is often locally enhanced by searchlight scattering, characterized in these data by the temporal rise in plume radiance measured by the broadside radiometer 2 in. downstream of the nozzle exit. This leads to an overestimate of the radiant heating from the near-field plume and of the axial decay rate (i.e. an underestimate of the plume length). Further complications can arise if the motor is spinning. In this case the plume tends to have a hollow core that grows as the burn progresses. This can lead to confusion regarding the time history of the radiant heating load, especially if there is only narrow field-of-view centerline radiometer coverage. On a previous spin-tested motor, for example, the narrow field-of-view centerline radiometer data showed a strong temporal variation, whereas the wide field-of-view radiometers did not. Lastly, the specification of the boundary for the equivalent hard body surface generally does not receive adequate consideration. This is an important parameter in the view-factor method because the net view factor between the plume and the payload scales roughly as the square of the plume divergence angle. To be conservative, the near-field plume boundary is often taken from the boundary of the luminous plume. This is sometimes an ambiguous procedure. In many instances the boundary is based upon overexposed video. This leads to a plume and a heating rate that are both too large. In actuality, thermal imaging measurements show that the plume has a considerable radial gradient, so that there is really not a well-defined edge at all.

3.2 SEARCHLIGHT EMISSION

3.2.1 Background

Searchlight emission has been identified as a strong contributor to the exit plane radiance of an exhaust plume. The searchlight effect refers to radiation emitted by the hot nozzle wall and internal flow, which subsequently illuminates the external particle flow. The

magnitude of the effect depends upon motor design, but searchlight generally leads to a large (e.g., factor of two) enhancement of the exit plane radiance. The need for understanding searchlight arises from the fact that it has a different axial decay rate and aspect angle dependence from the thermal plume radiation. The Bobco model extrapolates the downstream radiance levels in the plume assuming a single axial decay rate. Since there are actually two different decay rates, a rapid one for the searchlight and a slower one for the thermal component, the Bobco extrapolation is erroneous. This problem is generally aggravated by the fact that one is rarely able to observe more than 2 or 3 ft of exhaust plume in a typical altitude test cell, so that the existence of the two decay rates is not apparent. A similar problem occurs for the aspect angle dependence of the radiation. The searchlight is strongly angle-dependent, but the thermal emission is only mildly so. As a first approximation to the situation, one could say that the searchlight enhances only the broadside exit plane radiation while adding little to the thermal emission directed back towards the spacecraft. (This is partly attributable to the low efficiency of the exhaust particles for high-angle scattering.) Undiscerning application of calorimeter data, which must typically be taken broadside to the plume for practical reasons, therefore, leads to overestimation of the radiant heating rate.

3.2.2 Application and Results

Although a quantitative analysis of searchlight has not yet been performed on the data from these tests, clear indication of a strong exit plane searchlight can be seen. This is an important conclusion because the standard view-factor calculation of plume radiative heating cannot be performed on the radiance data until the searchlight is properly accounted for. The following section shows how the searchlight can be identified using the temporal and spatial variation of the data.

For rocket motors of sizes similar to the ones discussed in this report, the exhaust plume is optically thick with respect to scattering, but optically thin with respect to emission and absorption. This means that the thermal emission (roughly from 0.5- to 5-μm wavelength) from the plume will be roughly linearly proportional to the thrust, Th(t), and that radiation from the hot nozzle wall will be scattered and redirected with high efficiency [i.e., searchlight, Sl(t), will be important]. The temporal behavior of the radiance provides one indication of the importance of the searchlight term. Success was achieved with previous motor data by modeling the total emission, I(t), as a weighted sum of these two components.

$$I(t) = a(x) \times Th(t) + b(x) \times Sl(t) \tag{1}$$

The axial x dependence of the a and b coefficients is noted because the axial decay rate is generally faster for the searchlight component. This provides one means of identifying searchlight. The thrust term, Th(t), is measured during the motor firing. In general, the

searchlight term, Sl(t), looks like a slow rise to an asymptotic limit. It begins from 0 (i.e. cold nozzle wall) and reaches an asymptotic limit after several nozzle thermal relaxation time constants have elapsed. For similar motors, the searchlight term, Sl(t), was based upon calculations performed with the ACE code for ablating conducting materials (Ref. 6). Although this has not yet been done for the subject motors, a strong similarity in the final results is anticipated. During firings of similar motors, heating up of the nozzle lip required approximately 20 sec, leading to a slow, steady rise in exit plane signature over the first half of the burn. By midburn, the searchlight emission 5 in. downstream of the nozzle exit accounted for 70 percent of the total broadside radiance. Similar indications of searchlight emission can be seen for the subject motors. Figure 6 compares the normalized thrust and short wavelength infrared radiance time histories for the nonspin test, No. 2. The spin test is not considered here because of the additional temporal dependence introduced by the motor spin. The overall shape of the radiance versus time profile deviates significantly from the thrust profile and rises monotonically for the first 70 sec of the burn. The radiance profile is also smoother, with less frequency content. The thrust maxima at 10 and 35 sec, for example, are hardly discernible in the radiance profile. In this context, high frequency pertains to frequencies faster than the nozzle thermal time constant. The slow initial rise is attributed to a long thermal time constant of the nozzle. In the transform domain, one can consider Eq. (1) as defining the transfer function between the motor thrust and the radiance. Clearly, the thermal emission term, Th(t), has extremely high frequency response. Thus, if searchlight is small and a > > b, the net transfer function should have high frequency response. In fact, the opposite is true. The absence of high frequency components in the radiance profile indicates strong damping so that, at least within the constraints of the model, a < < b, and searchlight is the dominant effect at the exit plane.

The searchlight effect can also be identified by its spatial dependence. Monte Carlo radiative transfer calculations predict a rapid axial decay attributable to the combined effects of decreasing plume density, decreasing view factor between the nozzle and plume, and decreasing particle scattering efficiency at larger scattering angles. Since the relative contribution of searchlight drops with increasing axial distance, the characteristic ramping behavior of the searchlight should gradually fade away with increasing distance downstream of the nozzle exit. Figure 5 shows the broadside total radiometer data obtained at 2, 17, and 29 in. downstream of the exit plane. The character of the radiance time history curves shows precisely the behavior expected. At the 2-in. station, the ramping behavior is unmistakable; at 17 in. it is weaker; and at 29 in. it is difficult to discern and possibly even absent. In conclusion, the spatial and temporal behavior of the exit plane radiance is consistent with the behavior characteristic of a searchlight dominated situation.

11

3.3 ALUMINUM CHLORIDE ABSORPTION

3.3.1 Background

An absorption feature in the mid-UV spectra of the radiation from composite, aluminum-loaded solid-propellant rocket plumes has been observed from several measurements. This feature, which appears at about 261 nm and is about 4 nm wide, has been tentatively identified as aluminum chloride (AlCl) absorption bands. The bands were poorly resolved since they lie very close, as shown by the tabulation of the bands observed from electrical discharges given in Ref. 7. Aluminum chloride is predicted as one of the minor products of combustion from these propellants. If this feature could be measured at higher resolution, then the identity could be confirmed and the utility of the bands for diagnostic purposes investigated. This was the purpose for the measurements on the motors in this report.

3.3.2 Application and Results

The very deep UV absorption feature, typical of aluminum-loaded solid-propellant rocket plumes, as shown in Fig. 7, can be explained by the illustration of Fig. 8. The continuum radiation from the inner core aluminum oxide particulate plume passes through the underexpanded outer gas layer, and the radiation is selectively absorbed by the gas species, believed to be AlCl in this case.

During the spin test, the spectrometer was pointed directly toward the center of the plume. A typical spectrum is shown in Fig. 9. The spectral features clearly stand out. The tabulation of band heads given by Pearce and Gaydon (Ref. 7) is included here as Table 3. An analysis based on the information in Table 3 was performed and, with a small shift (0.34 nm) in the wavelength calibration, the identification given in Fig. 9 is almost perfect.

The maximum absorptance (or minimum transmission) at the AlCl band center was measured as a function of firing time to determine whether there was a dependence on the motor chamber pressure. This measurement was made by fairing in the continuum radiation to provide a source reference. The result is shown in Fig. 10. There does not appear to be a correlation with the chamber pressure in Fig. 4a.

During the nonspin test, the instrument was pointed at several angles to the normal in an effort to assess the effect of path length on the absorption and to see whether emission of the AlCl bands could be observed when viewing only the gas boundary. These data are shown in Fig. 11. The spectral features are still prominent for the scans near the plume axis but fade somewhat toward the boundary. No emission could be detected from the gas-only path. The transmission (minimum) is shown as a function of position in Fig. 12. Curiously,

the transmittance is smallest at the center and increases with the angle. At this point no explanation is available for this behavior.

3.4 SPIN EFFECTS

3.4.1 Background

The nozzle flow of a spin-stabilized rocket is actually a swirling flow, and this leads to observable perturbations of the external plume. The relevant nondimensional fluid mechanic parameter is the Rossby number, Ro, defined as the ratio of axial to swirl velocity. It is important to remember that, because of conservation of angular momentum, the swirl velocity in the nozzle throat is between 2 to 3 orders of magnitude faster than the motor spin rate, depending upon time during the burn. Rossby numbers for the subject motor near burnout are roughly 25 to 40, indicating a significant swirl effect.

Previous measurements on solid-propellant rocket motors at AEDC have exhibited a visible "dark core" region in the plume during spin testing of the motor. Analysis of the data from these motors has revealed a depression in radiance level at the plume centerline in radial plume profiles (Fig. 13). The figure shows development of the depression as the burn progresses. This phenomenon does not appear during firings of static motors and is therefore believed to result from the motor spin. Theories hold that the "dark core" is a spin-induced vortex that redistributes the aluminum oxide particles in the plume flow field, the vortex getting stronger as the burn progresses. The spin/nonspin nature of the test program discussed in this report provided a setting in which the spin influences on the plume could be studied.

3.4.2 Application and Results

Visible image data were acquired during both the spin and nonspin tests using two, gated cameras positioned side-on to the plume on orthogonal azimuths. The camera fields of view allowed imaging of the entire visible portion of the plume. To obtain radial intensity profiles, a vertical row of image pixels was digitized from the data for each test representing profiles approximately 12 in. downstream of the nozzle exit. Relative intensity profiles from each test are presented in Fig. 14. An artificially induced offset has been introduced in the data plots for clarity between the time-dependent curves. Notice the centerline depression apparent in the data from the spin test that is not present in the nonspin data. Also notice how the depression seems to get deeper with time. Although the spin effects are slightly smeared out by the line-of-sight integration implicit in the imaging process, the results strongly support the spin-induced vortex theory concerning the "dark core" phenomenon observed in spin-tested motors. The full extent of the spin effect upon the plume structure can be ascertained only after Abel inversion of the data.

13

3.5 PARTICLE MASS DISTRIBUTION

3.5.1 Background

A laser beam is attenuated when it passes through a rocket motor exhaust plume. If the wavelength of the laser is in a portion of the wavelength spectrum where the gases are nonabsorbing, the attenuation is caused by light being scattered out of the beam and absorbed from the beam by solid and liquid particulates. One would expect that, generally, attenuation would be greatest where particle number density is greatest, or if particle number density were uniform throughout the exhaust flow, then one would expect more attenuation the bigger the particles since larger particles have larger cross-sectional areas to intercept more of the beam. In fact, the amount of beam attenuation depends both on the particle number density and on the size of the particles relative to the wavelength, in addition to other factors such as the shapes of the individual particles and their index of refraction.

Light beam attenuation, or "extinction," is mathematically quantified as follows. The intensity, I, after the beam has passed a distance L through a cloud of particles is given by

$$I = I_0 e^{-\tau} \tag{2}$$

where I_0 is the initial beam intensity and τ is the "optical density" given by

$$\tau = kL \tag{3}$$

where k is the extinction coefficient. In making a beam intensity measurement, it is assumed that the receiver optics have sufficiently small collection angle so that only a negligible portion of light is detected that has been once scattered out of the beam and then rescattered in the direction of the detector. Since scattering and absorption can be calculated for spheres using Mie-Lorenz theory, and because the aluminum oxide particles in rocket exhaust probably are spherical, it is usually further assumed that we are dealing with spheres. The following expression can be derived for the extinction coefficient (Ref. 8):

$$k = \frac{3c_m <Q_e>}{2\,\varrho\,D_{32}} \tag{4}$$

where c_m is the plume mass concentration (grams of particulate per cm^3 of plume), ϱ is the particle material density (gm/cm^3), D_{32} is the Sauter mean diameter of the particle size distribution, and $<Q_e>$ is the mean extinction efficiency, calculated from Mie theory and dependent on the particular size distribution. Empirical studies have shown that this relation for k is relatively insensitive to uncertainty in particle shape or refractive index.

Equation (4) relates the extinction coefficient k, which may be determined through a laser transmission measurement via Eq. (2), to c_m, $<Q_c>$, and D_{32}. These three parameters are all functions of the generally unknown particle size distribution. Additional study will be required to determine what information concerning these parameters and the underlying size distribution can be extracted from a measurement of k.

Transmission measurements along several paths through the plume, as shown in Fig. 15, can be used to obtain a radial profile of the plume extinction coefficient. The procedure for determining the extinction coefficient radial profile involves dividing an axisymmetric particle cloud into N annular regions, each of which is assumed to have a uniform particle size distribution. Transmission measurements are made for each of N parallel paths through the particle cloud, with the number of annular regions equal to the number of measurement paths. Data are acquired over only half of the circular cloud since it is assumed to be symmetrical.

3.5.2 Application and Results

Two neodymium yttrium aluminum garnet (Nd:YAG) lasers were used to measure plume transmission at 0.532 and 1.06 μm for the spin-tested motor and at 1.06 μm for the nonspin motor. The two Q-switched lasers provided eight beams pulsed at 1,000 pulses/sec, which were transmitted to the test cell using eight, 400-μm core diameter fiber-optic cables. The arrangement in Test Cell J-5 is shown in Fig. 16. Illumination probes located close to the cell wall projected eight parallel beams through the plume to collection optics located on the opposite wall. Frequency doubling crystals were used during the spin test to provide coincident 0.532- and 1.06-μm beams carried along the same paths. The system was self-calibrating with the prefire signal defining 100-percent transmission and a fully blocked beam defining 0-percent transmission.

Transmission data were taken with the Nd:YAG system at both 1.06- and 0.532-μm wavelengths during the spin test. A problem occurred when steam was injected into the cell just prior to motor firing, which obscured the signals during the time when they were to be calibrated at 100-percent transmission. A calibration was later obtained for some of the data, namely that for Paths 2, 4, 6, and 8 at 1.06 μm and Paths 2, 4, and 6 at 0.532 μm, by measuring 100-percent signal transmission after the test. However, the optics for the other paths had been disturbed before the problem was recognized and a calibration could not be obtained. The calibration problem was rectified for the nonspin test by measuring 100-percent transmission at a time well before steam was injected into the cell, and acceptable laser transmission data were obtained during that test at 1.06 μm. Plots of transmission, I/I_o, versus time for the 1.06 μm data, which are typical of the Nd:YAG laser data acquired during this test, are presented in Fig. 17. Path Numbers 1, 3, 5, and 7 pass at distances of approximately 2.5, 8.1, 13.7, and 19.1 in. from the plume centerline, respectively.

15

Results from calculation of the extinction coefficient radial profile using the eight, 1.06-μm transmission paths from the nonspin test are shown in Fig. 18. The transmission data used in the calculation were acquired at approximately 50 sec into the motor burn. The calculated extinction profile from the four paths at 1.06 μm for the spin test is presented in Fig. 19. The time of this profile was also approximately 50 sec into the motor firing.

As can be seen from Eq. (4), the extinction coefficient depends directly on c_m, the plume mass concentration, but it also has a dependence on the distribution of sizes in the particulate cloud as reflected in the factor $<Q_e>/D_{32}$. It cannot be assumed that regions of varying beam extinction coefficient in the plume necessarily mean a proportionate variation in mass concentration. Additional work is necessary to determine how much information regarding the particulate size distribution can be extracted from the extinction coefficient measurements.

4.0 SUMMARY AND RECOMMENDATIONS

Plume diagnostic measurements were acquired during firing of two identical solid-propellant rocket motors designed to provide perigee kick performance for payload orbital transfer. Both motors were fired under simulated altitude conditions of approximately 100,000 ft. One motor was spin-tested, and the other was static-tested. The measurements were made to investigate plume phenomena useful in characterizing solid-propellant rocket plumes. Limited initial analysis of the data has been performed, and results are reported as they apply to plume heat-transfer calculations, searchlight emission, AlCl absorption, spin effects, and aluminum oxide particle distribution within the plume.

Radiant heating calculations for these motors have not yet been done. Once the searchlight contributions are removed from the radiometer data, however, a good indication of the axial decay rate and resulting plume shape should be revealed and will be used as an input into specification of the boundary for the equivalent hard body surface. The radiance data show a strong aspect angle dependence characterized by the low radiance levels detected by the downstream viewing radiometer. These data should prove very useful in overcoming the overestimation of radiant heating calculated by present models.

The motor seems to exhibit a large searchlight component in the plume radiance. Temporal characteristics of searchlight are evident in the slow rise in plume radiance as compared with the motor thrust curve. A lack of high frequency components in the radiance curve is also indicative of searchlight contributions. The spatial dependence of searchlight is shown by the gradual fade of the ramping behavior of the searchlight with increasing axial distance downstream of the nozzle exit. Further analysis is required to quantify the searchlight component of the plume radiance so that correct radiant heating predictions can be made.

The absorption feature in the mid-UV spectra from aluminized solid-propellant rocket plumes has been positively identified as arising from AlCl. The feature has a deep absorption ranging from 15 to 20 percent during the firing. The results are approximately the same whether the motor is being spun or not. The feature changes in depth as the angle between the normal to the axis increases and the line of sight increases, but the spectral features remain. The analysis carried out so far on these data has been meager. It remains to model the radiative transfer path using a line-by-line spectral calculation to determine whether the data can be used to determine temperature and concentration of the AlCl.

Theories attributing the "dark core" phenomenon apparent in some spin-tested motors to a spin-induced vortex are supported by the data. The spin-versus-nonspin nature of the tests allows direct comparison of data from the two identical motors. Motor spin causes a vortex to form within the plume that gets stronger with time as evidenced by the centerline depression in the spin data, which deepens as the burn progresses. The depression is not apparent in the nonspin data. Although the image data support the vortex theory, Abel inversion of the data would reveal the full effects of motor spin on the plume structure.

Radial profiles of extinction coefficients have been calculated from the laser transmission measurements for both the spin and nonspin motors. The extinction coefficient, however, is dependent on the plume mass concentration and on the distribution of sizes in the particulate cloud. Therefore, variations in beam extinction coefficient in the plume do not necessarily coincide with proportionate variations in mass concentration. Additional work is required to determine the exact relationship between these parameters.

REFERENCES

1. Zakin, M. R., Duff, J. W., and Bernstein, L. S. "CHARM Searchlight Scattering and Particle Thermal Emission Model." SSI-TR-155, Spectral Sciences Inc., Prepared for the Air Force Astronautics Laboratory, Edwards AFB, July 1989.

2. Limbaugh, C. C. "The Infrared Emission-Absorption Method for Temperature and Species Partial Pressure Determination in Flames and Plumes." *Infrared Methods for Gaseous Measurements, Theory and Practice*, Edited by Joda Wormhoudt, New York and Basel, 1985.

3. Greenwood, T. F. et al "Calculation of Shuttle Base Heating Environment and Comparison With Flight Data." *Shuttle Performance: Lessons Learned*, NASA Conference Publication 2283, 1983.
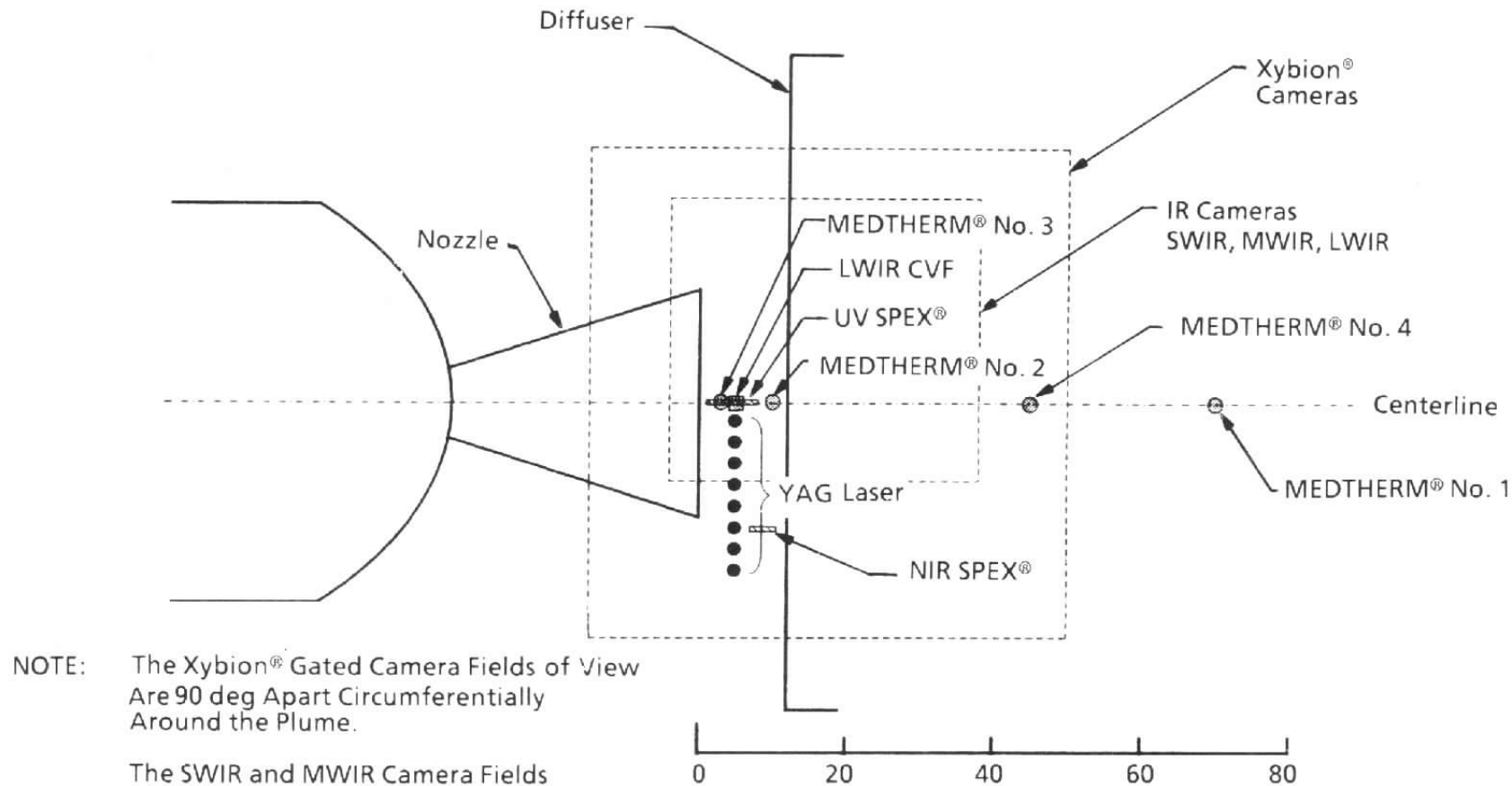
4. Edwards, D. K. and Bobco, R. P. "Effect of Particle Size Distribution on the Radiosity of Solid Propellant Rocket Motor Plumes." AIAA Paper No. 81-1052, AIAA 16th Thermophysics Conference, 23-25 June 1981, Palo Alto, California.

5. Edwards, D. K., Sakurai, Y., and Babikian, D. S. "A Two-Particle Model for Rocket Plume Radiation." *AIAA Journal of Thermophysics*, Vol. I, No. 1, January 1987.

6. "An Analysis of the Coupled Chemically Reacting Boundary Layer and Charring Ablator." NASA CR-1060 through CR-1065, Parts I—VI, Prepared by ITEC Corp., Vidya Division, for the Manned Spacecraft Center, NASA, 1966.

7. Pearse, R. W. B. and Gaydon, A. G. *The Identification of Molecular Spectra*. Chapman and Hall Ltd., London, 1950.

8. Cashdollar, K. L., Lee, C. K., and Singer, J. M. "Three-Wavelength Light Transmission Technology to Measure Smoke Particle Size and Concentration." *Applied Optics*, Vol. 18, No. 11, June 1979.
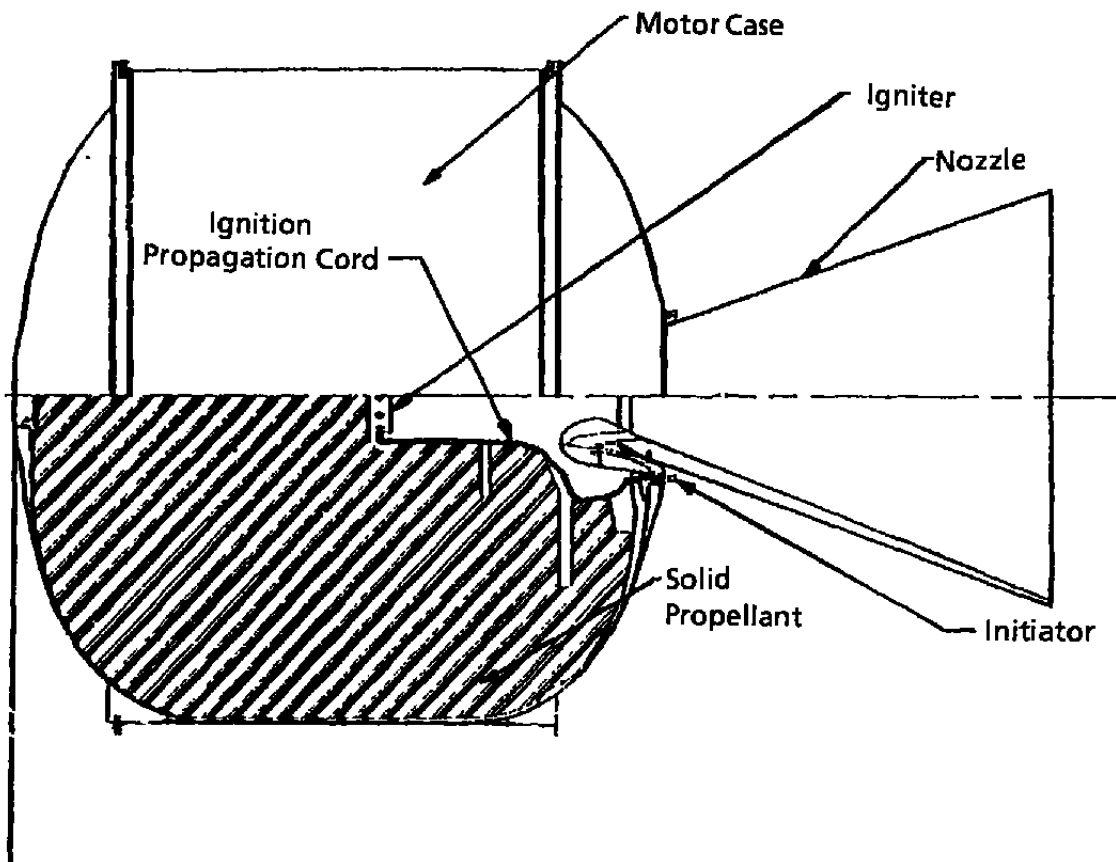
Figure 1. Typical perigee kick solid-propellant rocket motor.

Auxiliary Pumping System (1 of 2)

102-in.-diam Diffuser (Water Cooled)

Exhaust Diffuser (Water Cooled), 102-in.-diam Entrance; Tapers to 84-in.-diam Throat Section

Test Article (Spin Motor)

Air-Conditioning Duct (1 of 2)

Loading Hatch

Thrust Calibrator

First-Stage Steam Ejector

Main Steam Ejector

Test Cell J-5 - 16-ft Diameter by 50 ft Long

Thrust Abutment
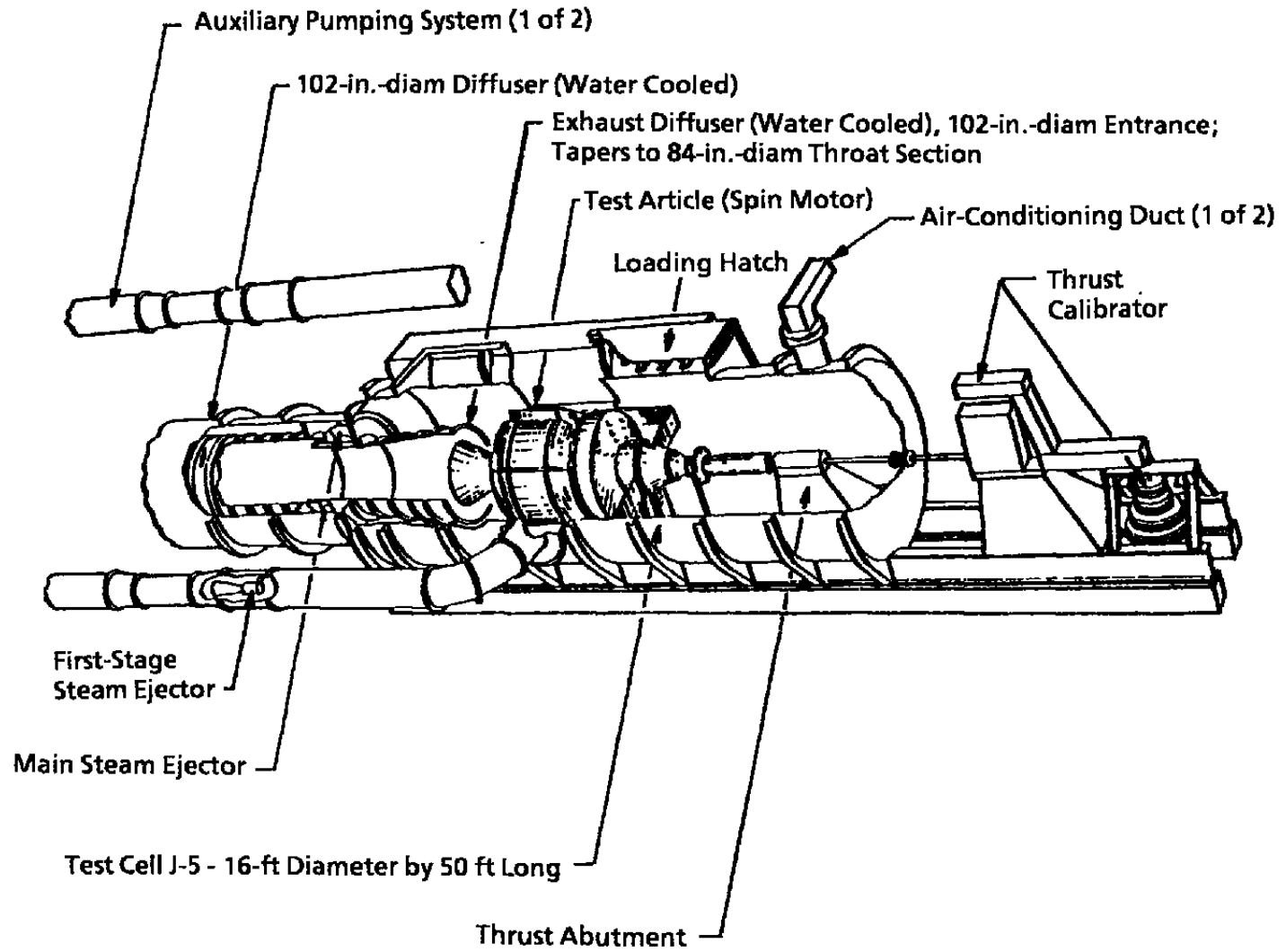
Figure 2. Rocket Development Test Cell J-5.

NOTE: The Xybion® Gated Camera Fields of View Are 90 deg Apart Circumferentially Around the Plume.

The SWIR and MWIR Camera Fields of View Coincide. The LWIR Camera Field of View Is Offset Approximately 120 deg Circumferentially Around the Plume.

a. Spin motor
Figure 3. Instrument fields of view.
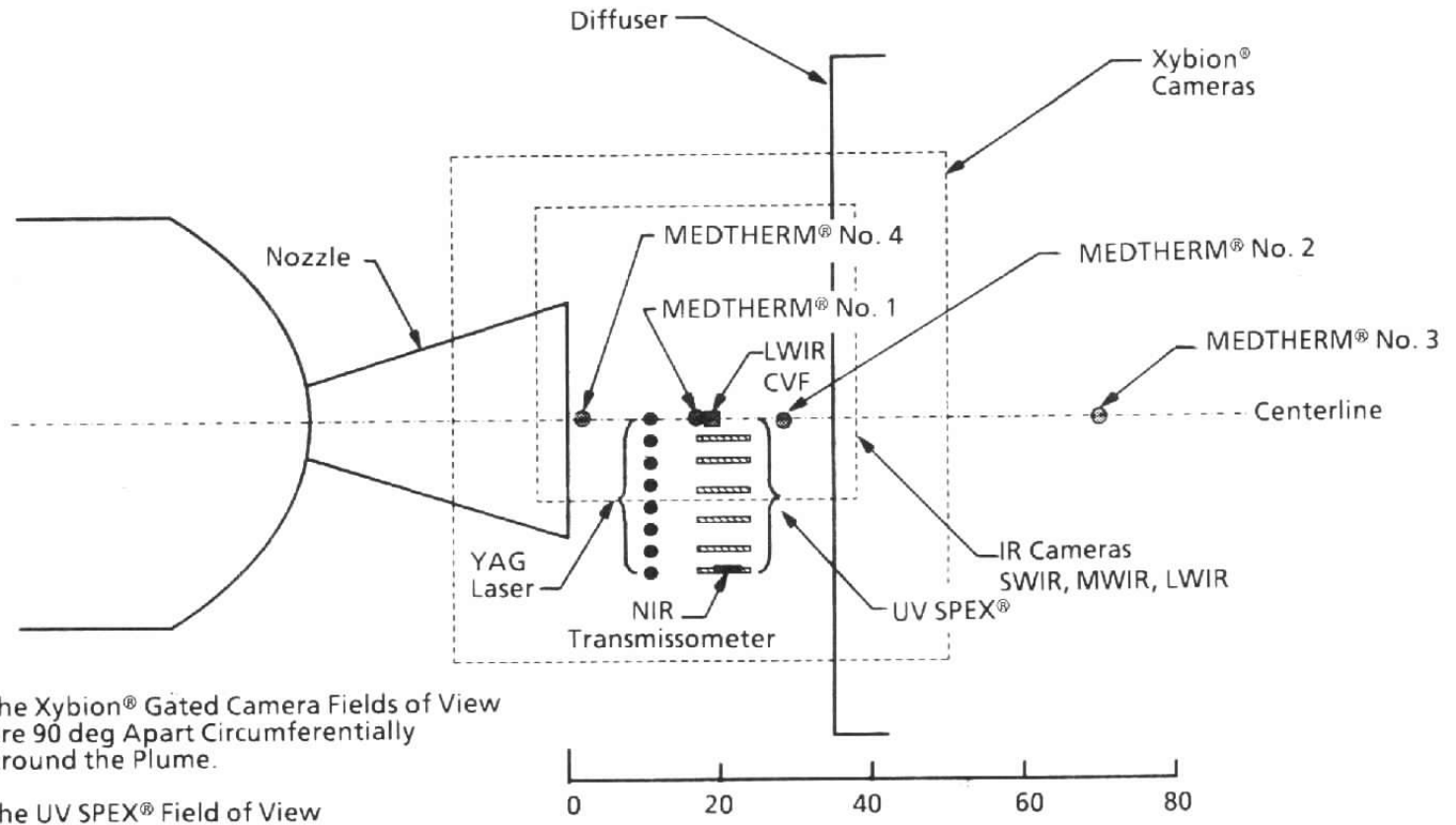
NOTE: The Xybion® Gated Camera Fields of View Are 90 deg Apart Circumferentially Around the Plume.

The UV SPEX® Field of View Moved to the Indicated Locations During the Firing, the First Position Being Farthest from the Centerline.

b. Nonspin motor
Figure 3. Concluded.
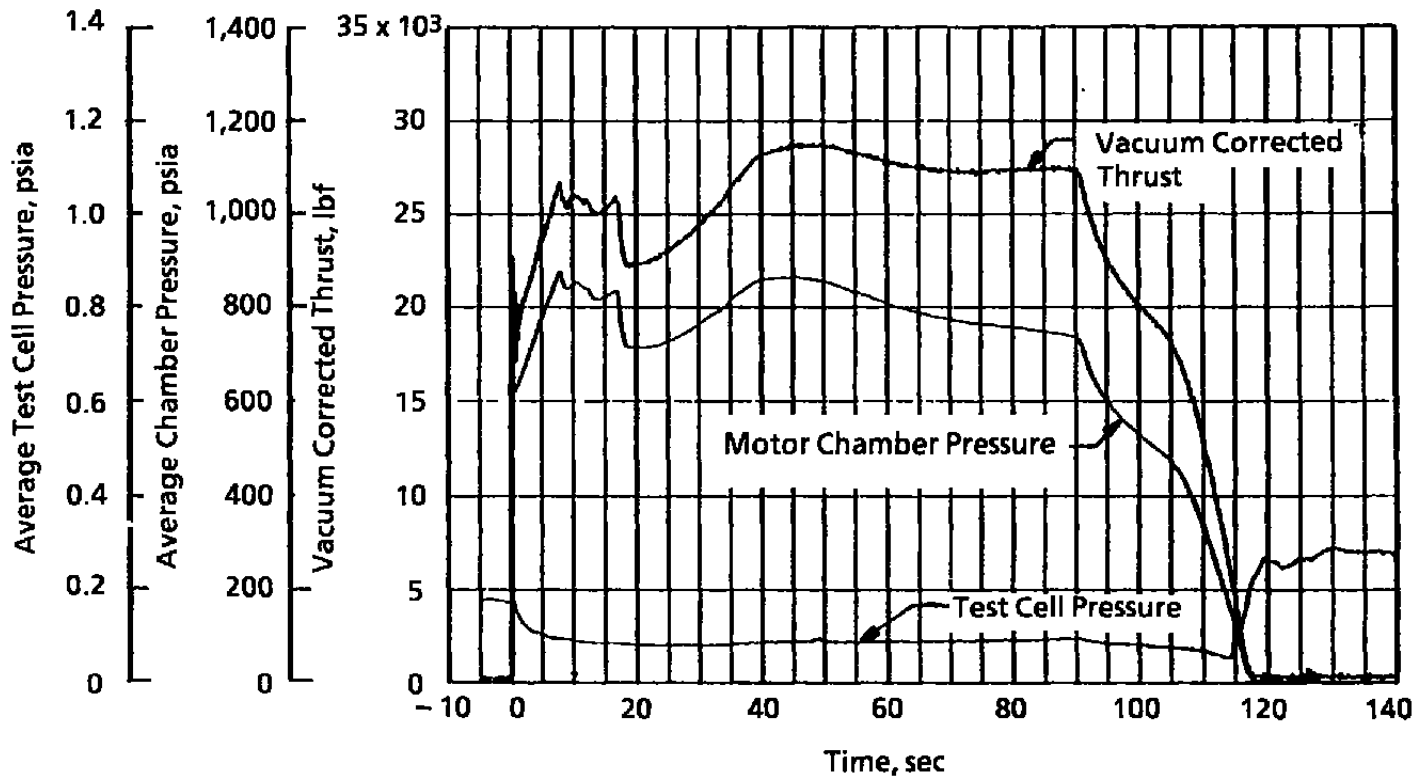
a. Spin motor
Figure 4. Motor and test cell performance.
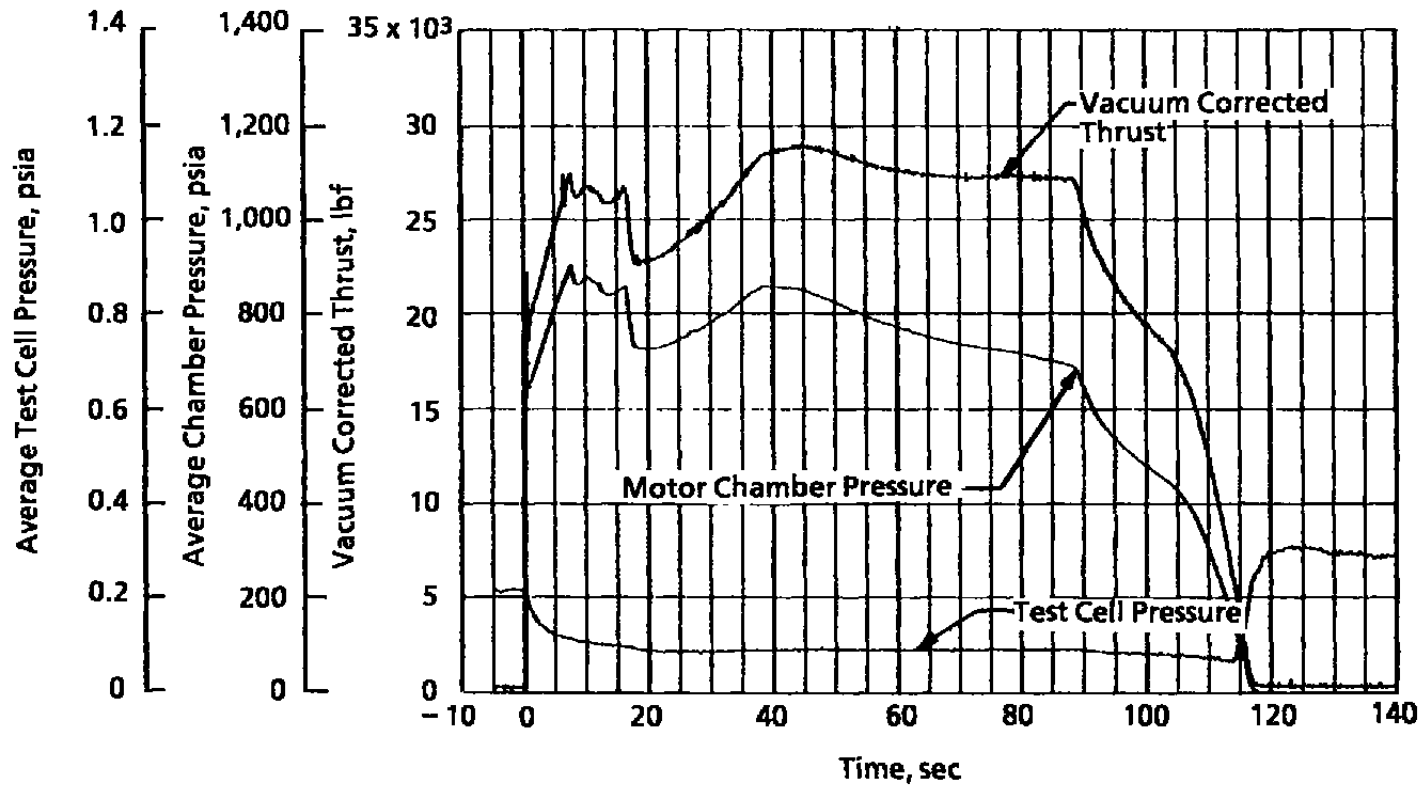
b. Nonspin motor
Figure 4. Concluded.
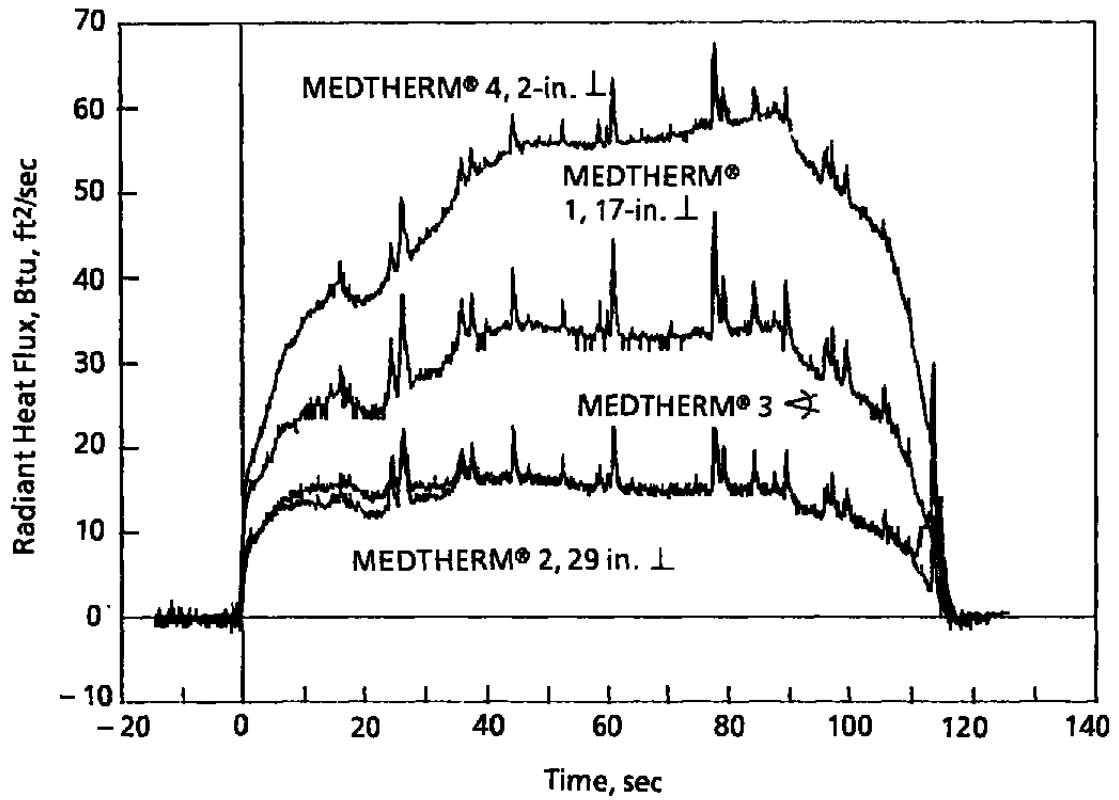
Figure 5. Composite plot of total radiometer heat flux data, nonspin motor.
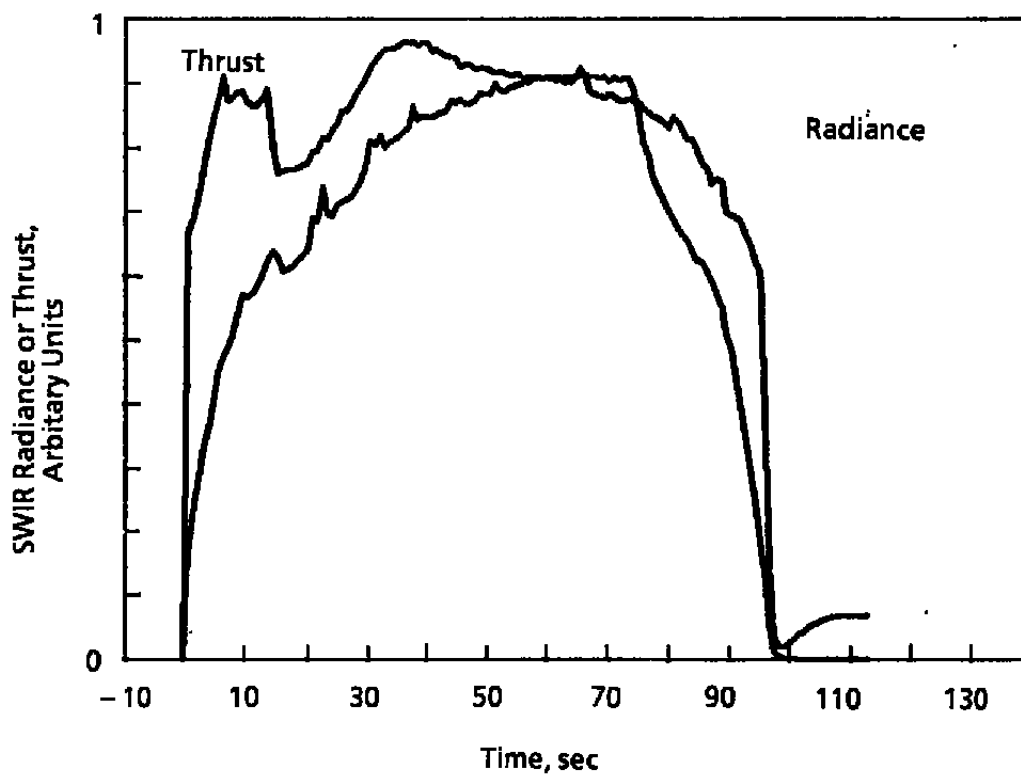
Figure 6. Normalized thrust and SWIR radiance time histories.
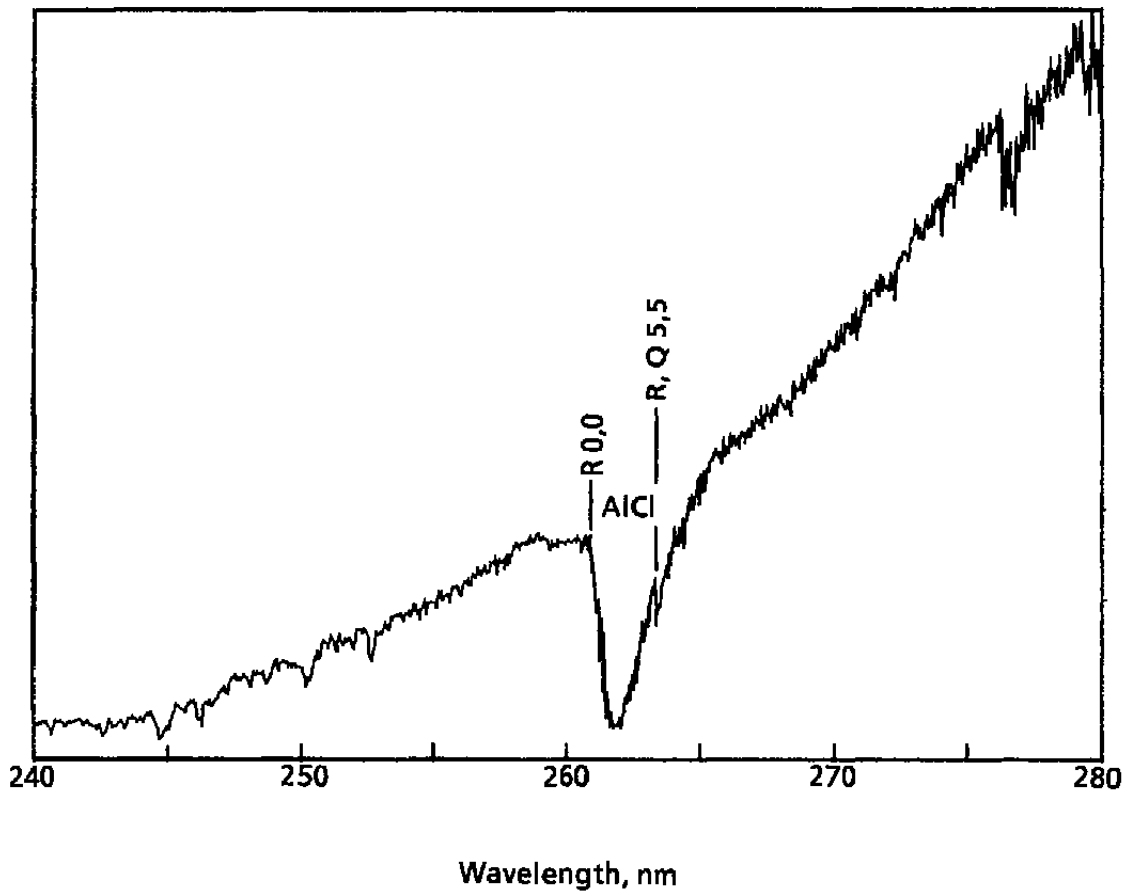
Figure 7. Typical mid-UV spectra from solid-propellant rocket motor plume.
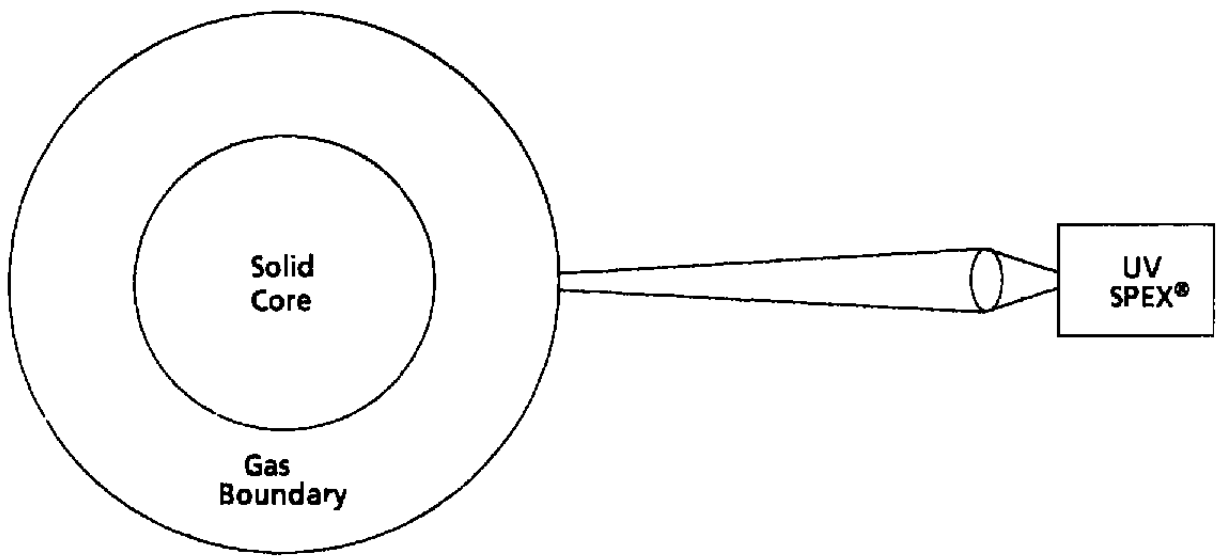
Figure 8. UV spectrometer measurement technique.
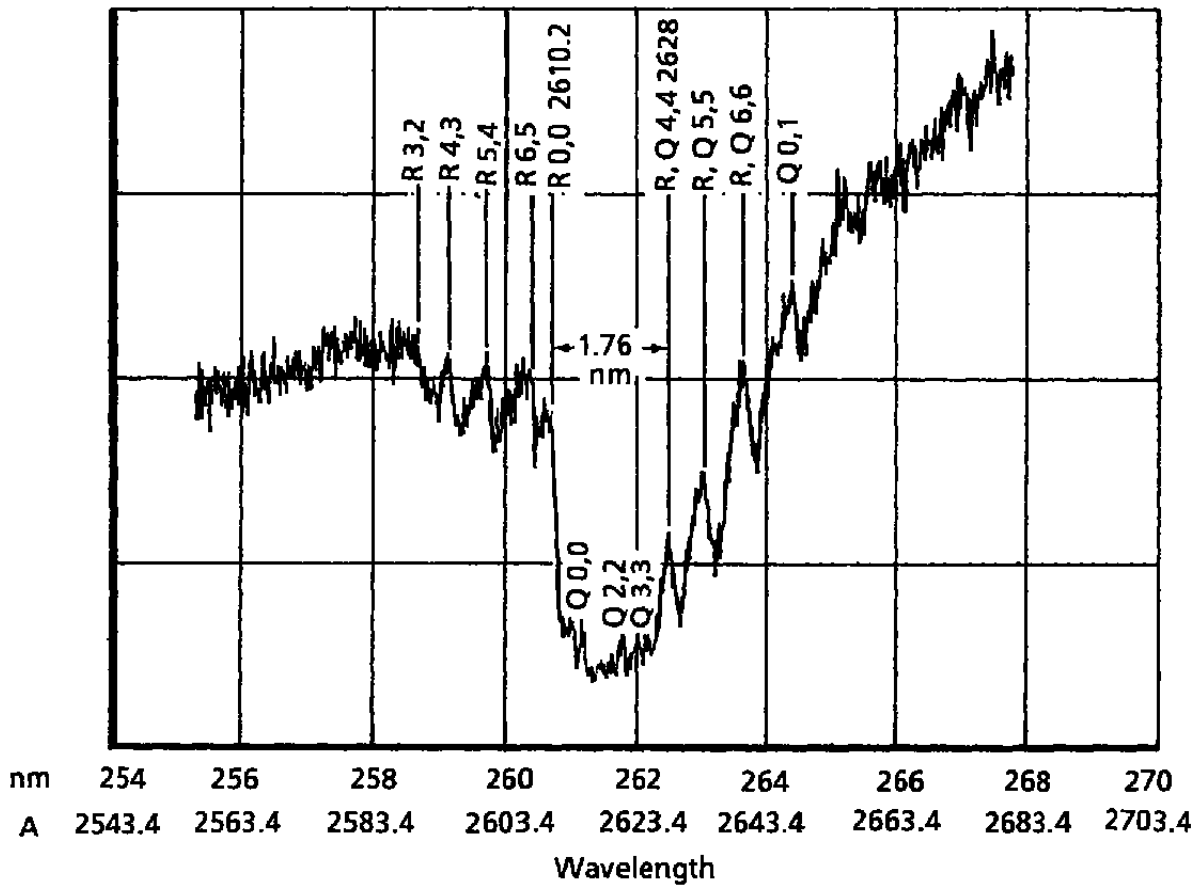
Figure 9. Typical UV plume spectra with absorption bands.
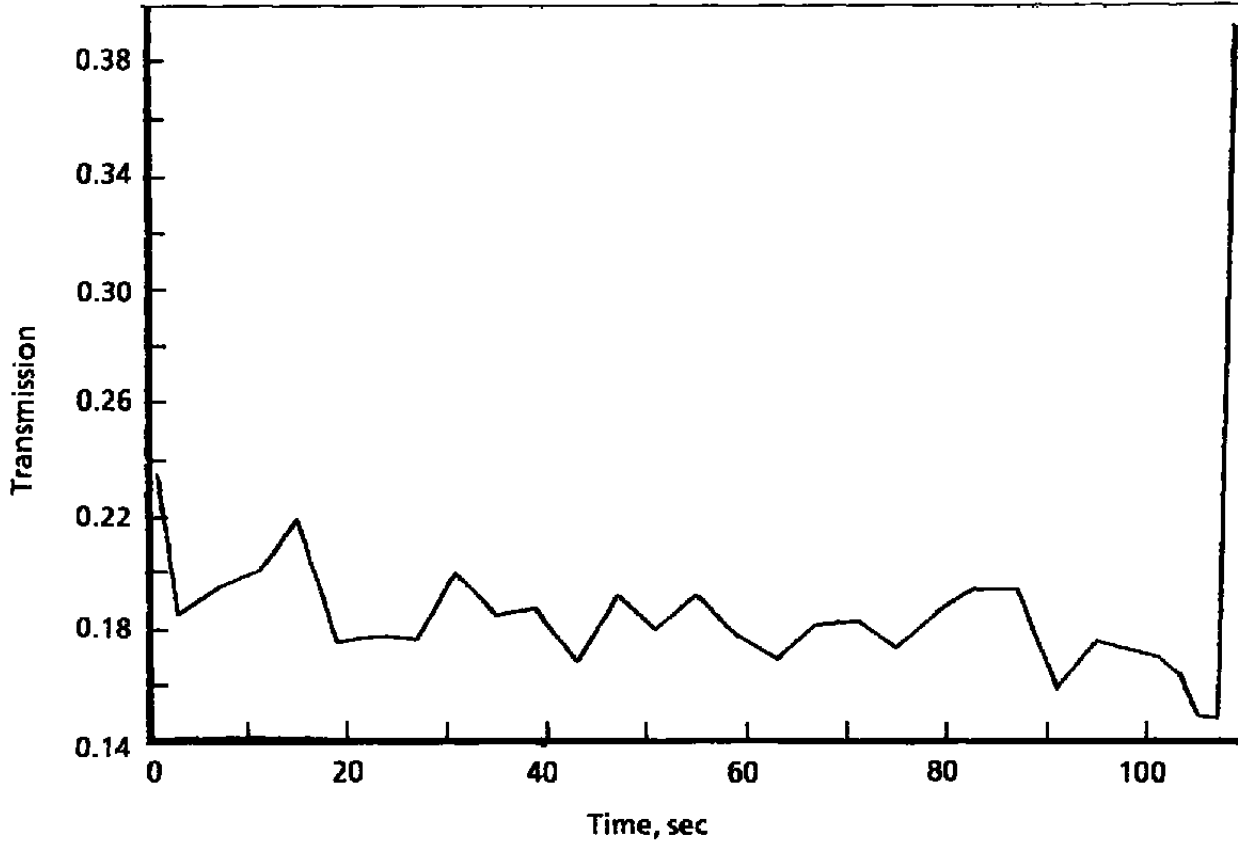
Figure 10. UV plume transmission time history, spin motor.
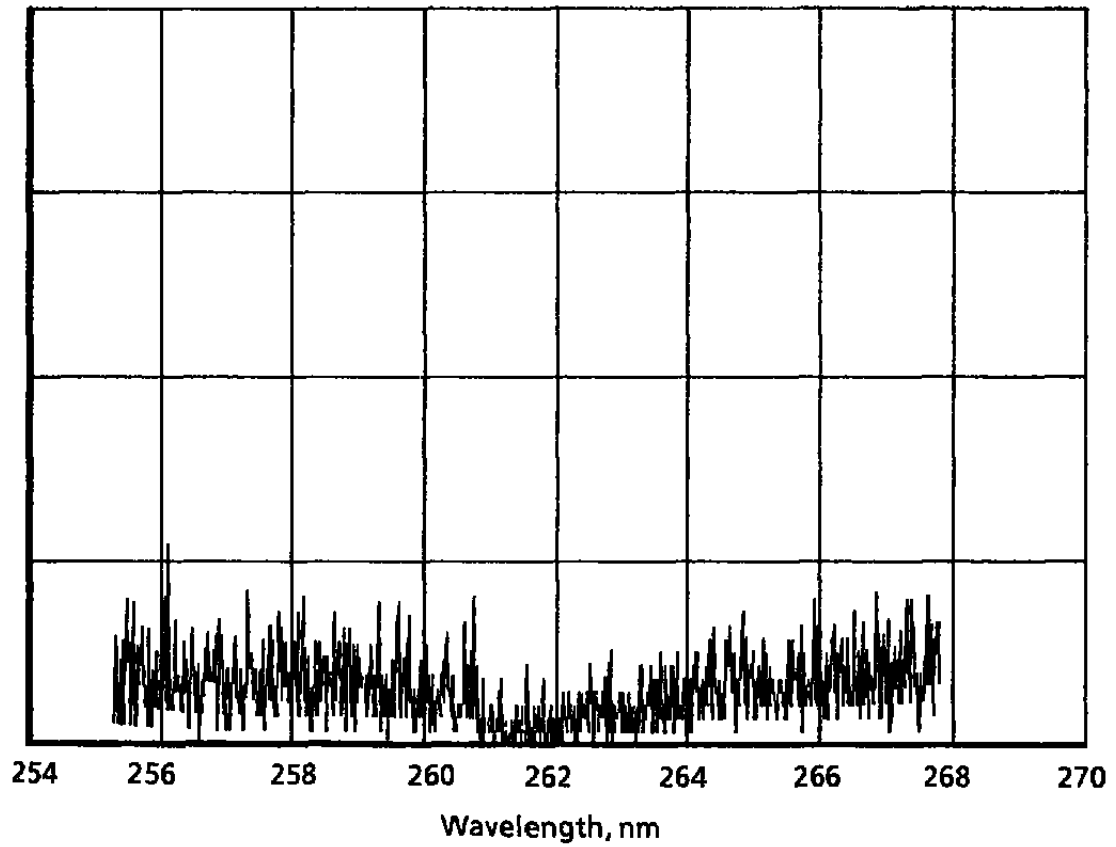
a. Position 1, r = 22.0 in.
Figure 11. UV plume spectra, nonspin motor.
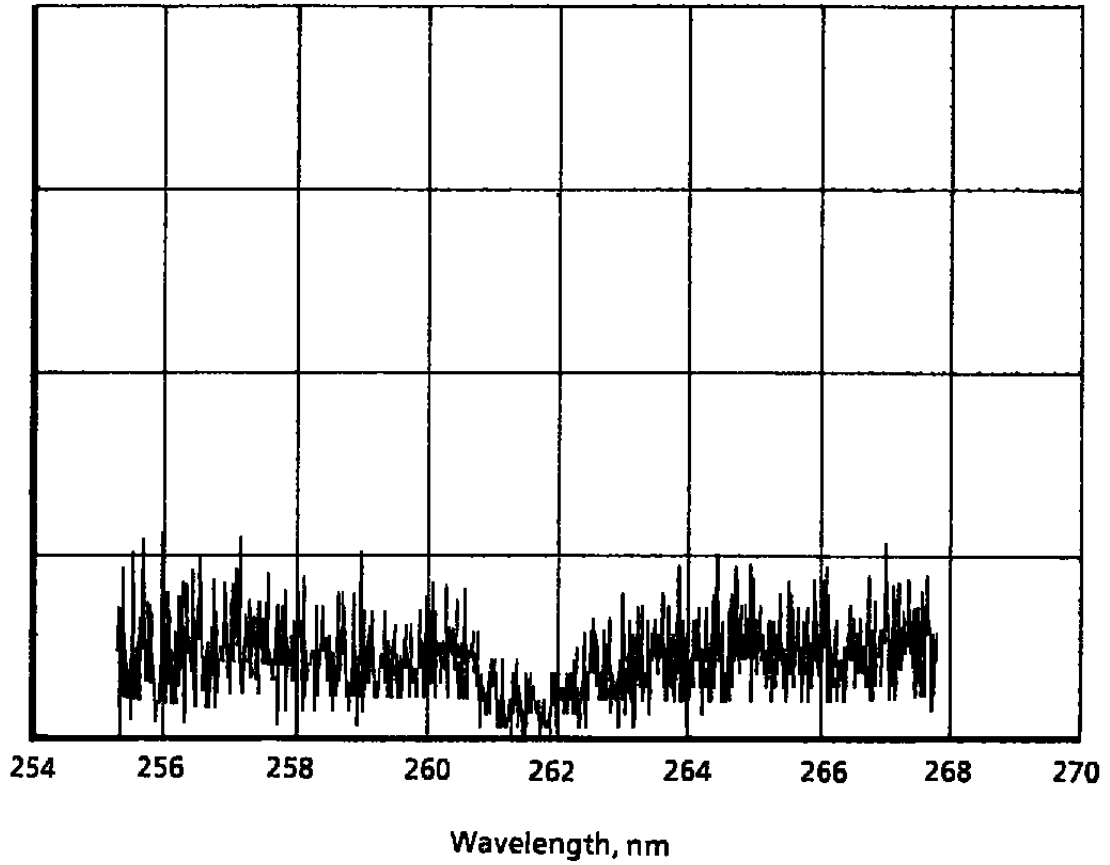
b. Position 2, r = 18.2 in.
Figure 11. Continued.

Wavelength, nm
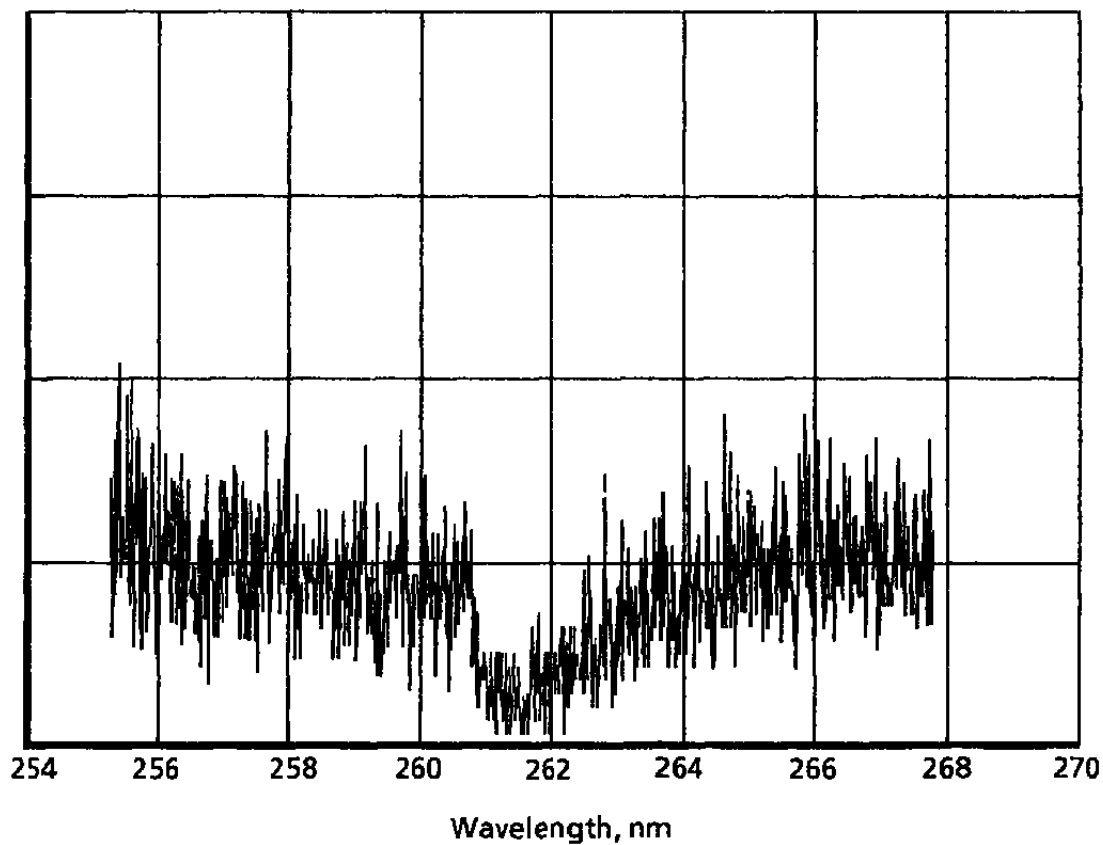
c. Position 3, r = 14.4 in.
Figure 11. Continued.
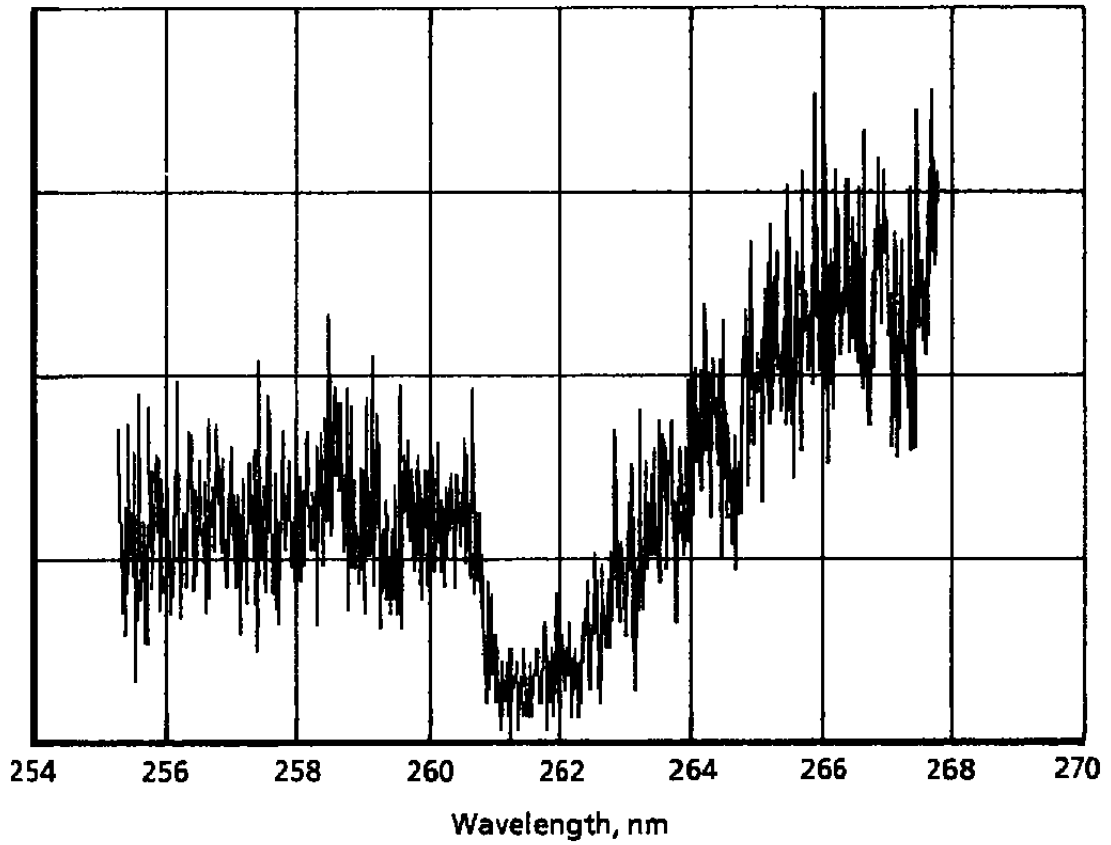
d. Position 4, r = 10.6 in.
Figure 11. Continued.
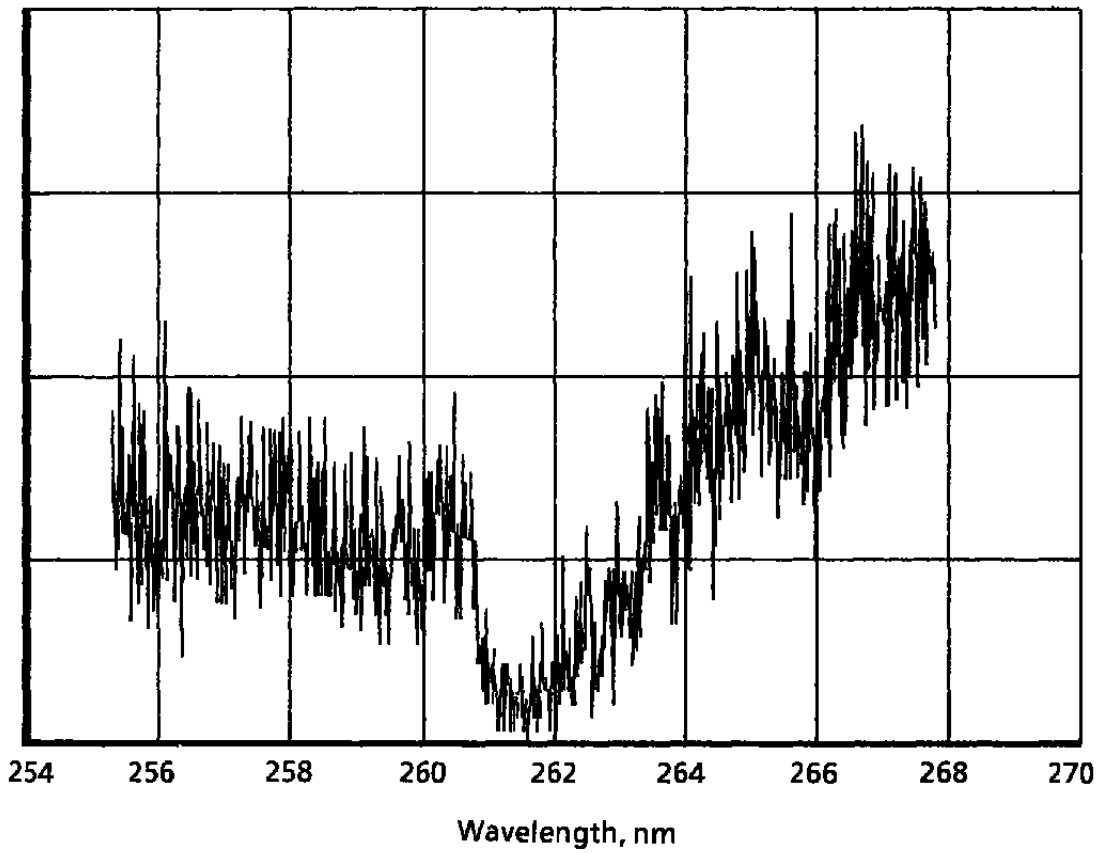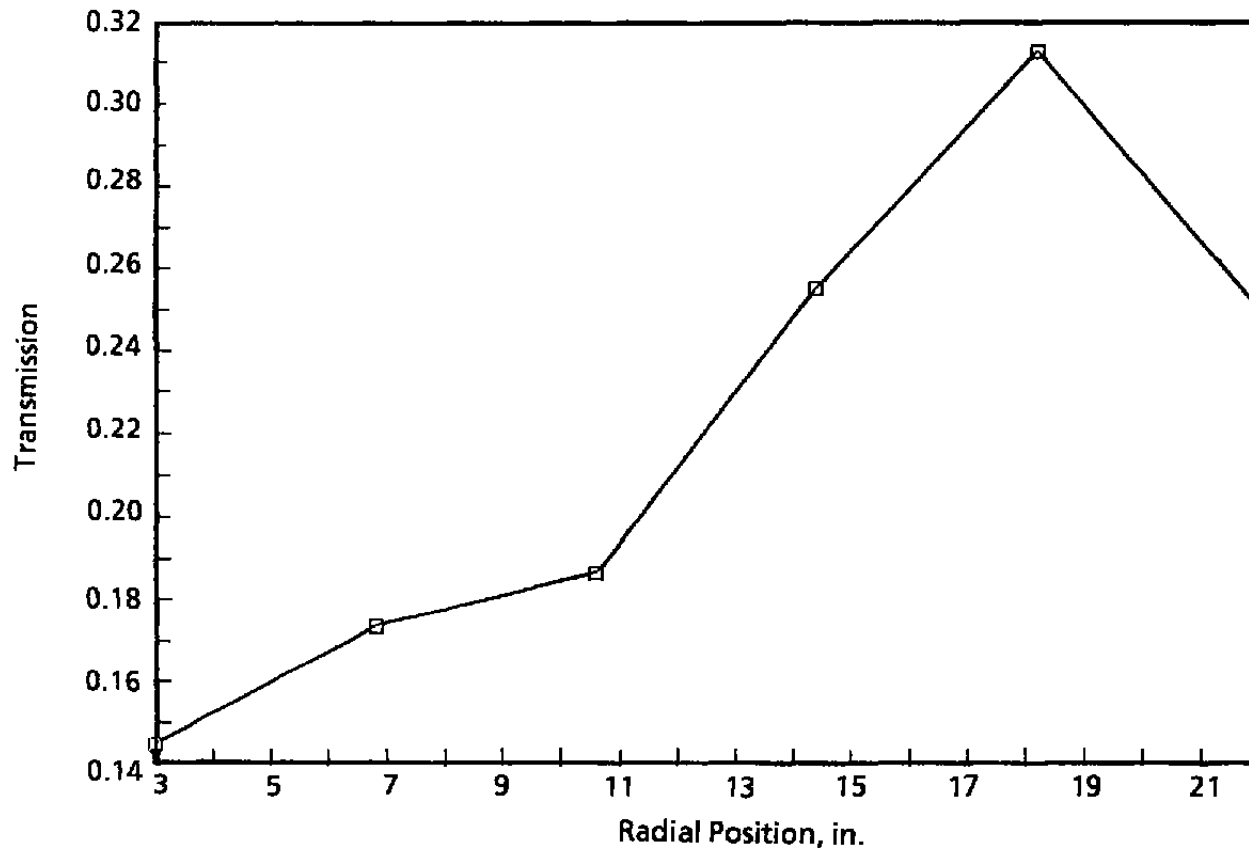
e. Position 5, r = 6.8 in.
Figure 11. Continued.
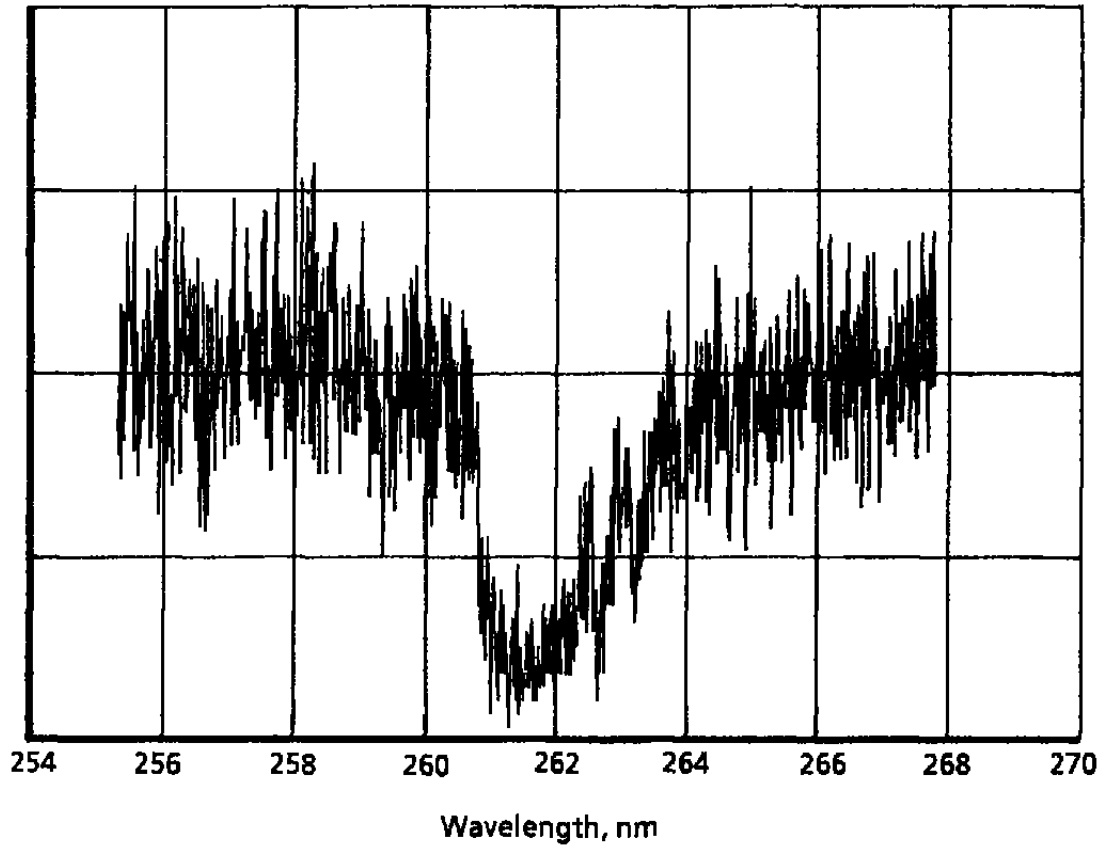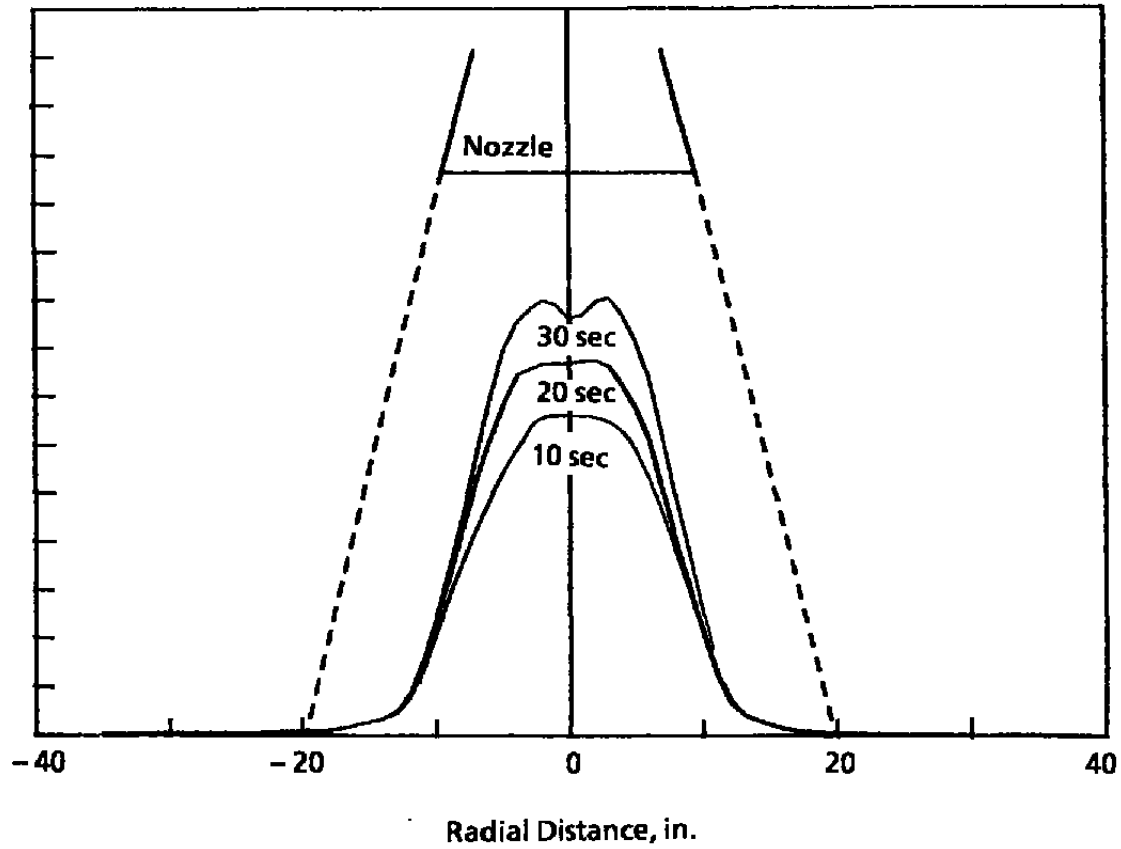
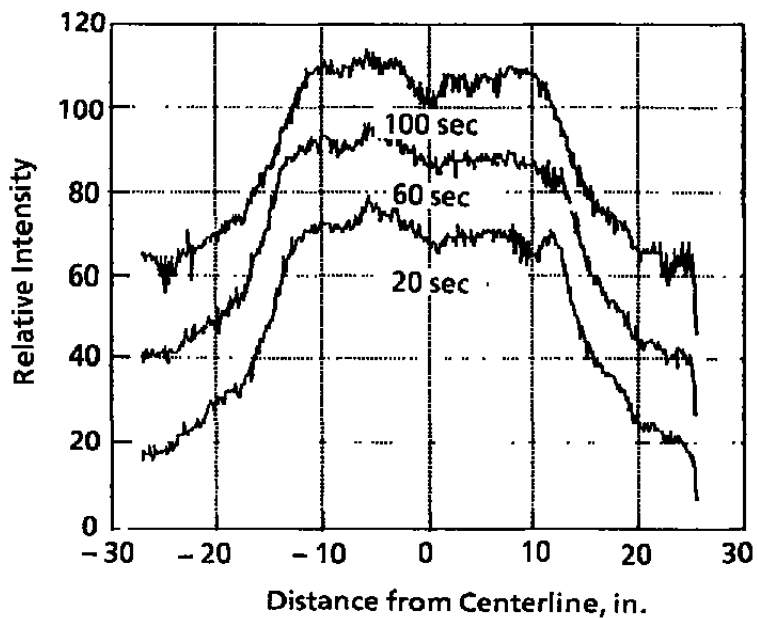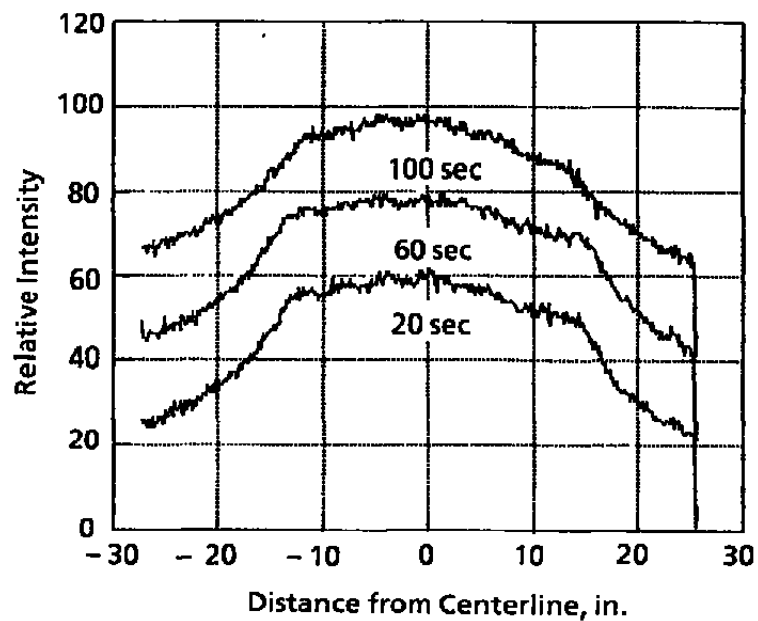f. Position 6, r = 3.0 in.
Figure 11. Concluded.

Figure 12. UV plume transmission versus radial position, nonspin motor.

Figure 13. High aluminum content solid-propellant rocket motor plume radiance profiles.

Radial Distance, in.

a. Spin motor

b. Nonspin motor

Figure 14. Relative intensity profiles showing spin effects.

Optical Depth

$$\tau_i \quad \sum_{j=1}^{N} \tau_{ij}$$

i   Path
j   Ring
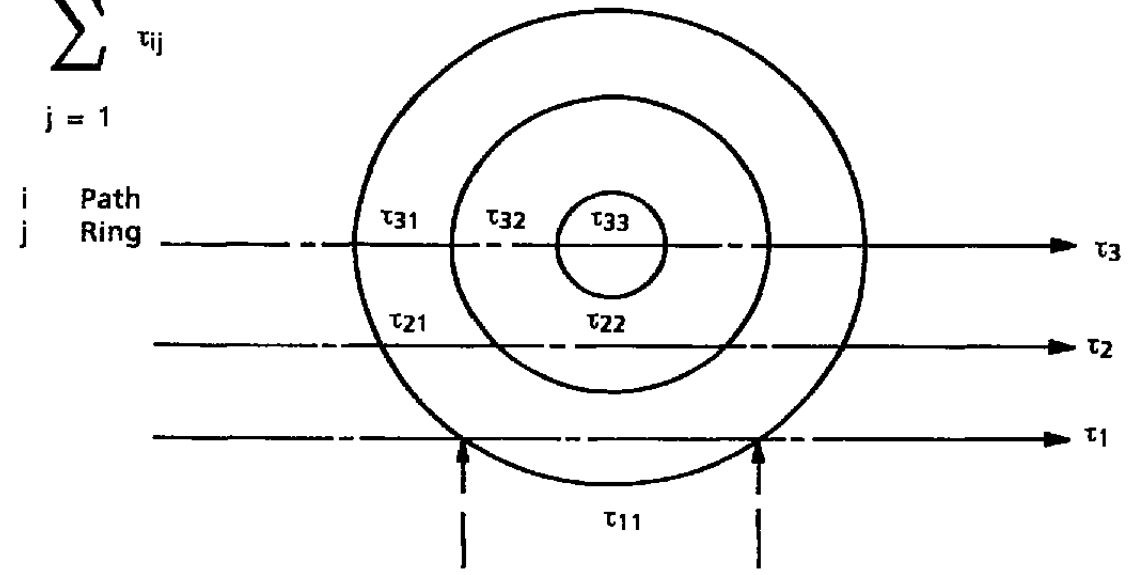

Figure 15. Extinction measurements along several paths through the plume.

Plume

Nozzle

Diffuser
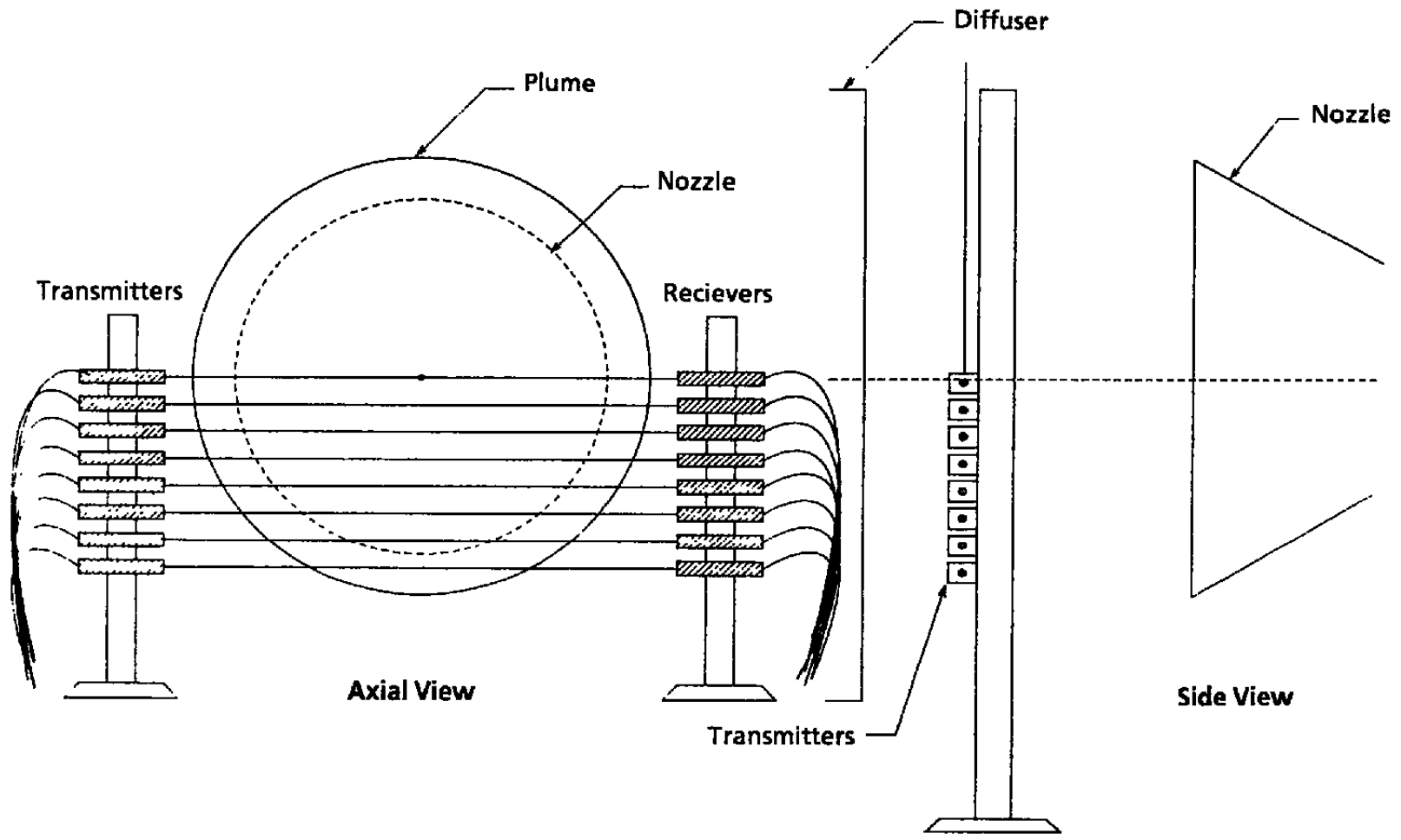
Nozzle

Transmitters

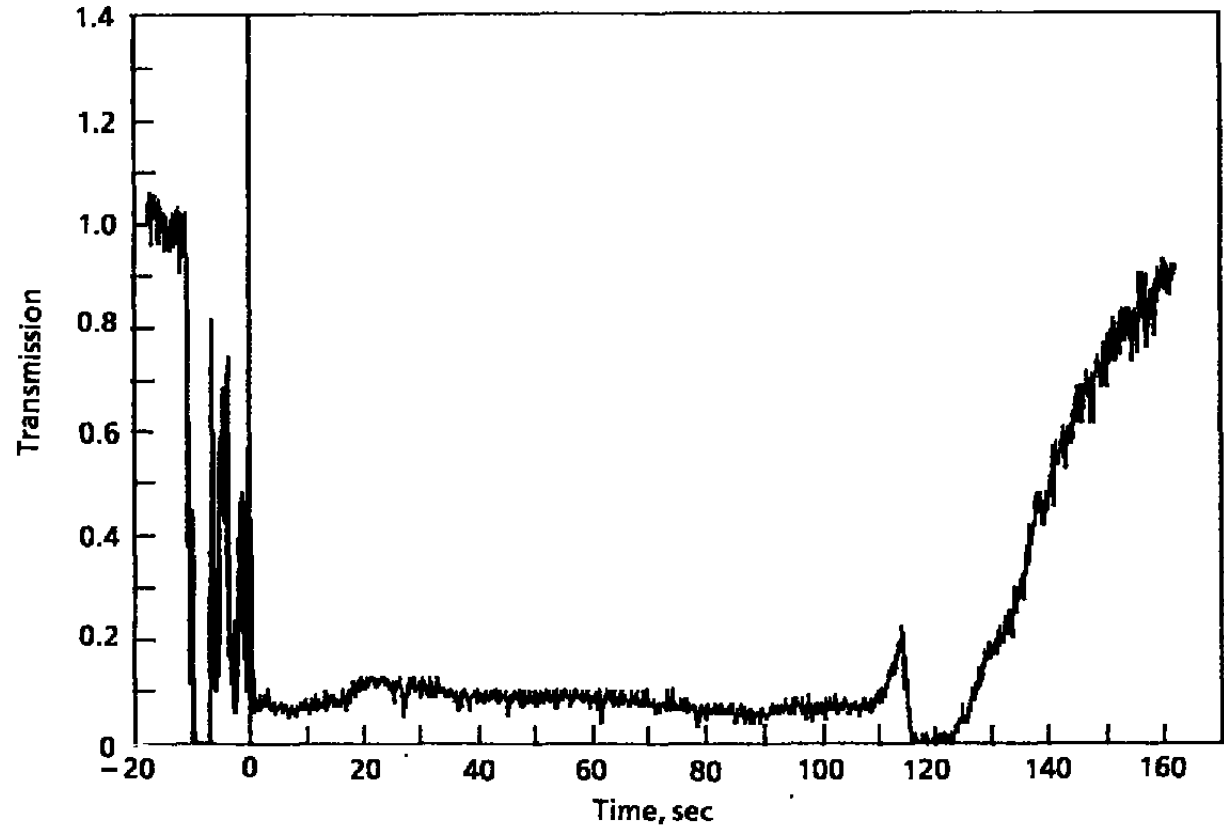Recievers

Axial View
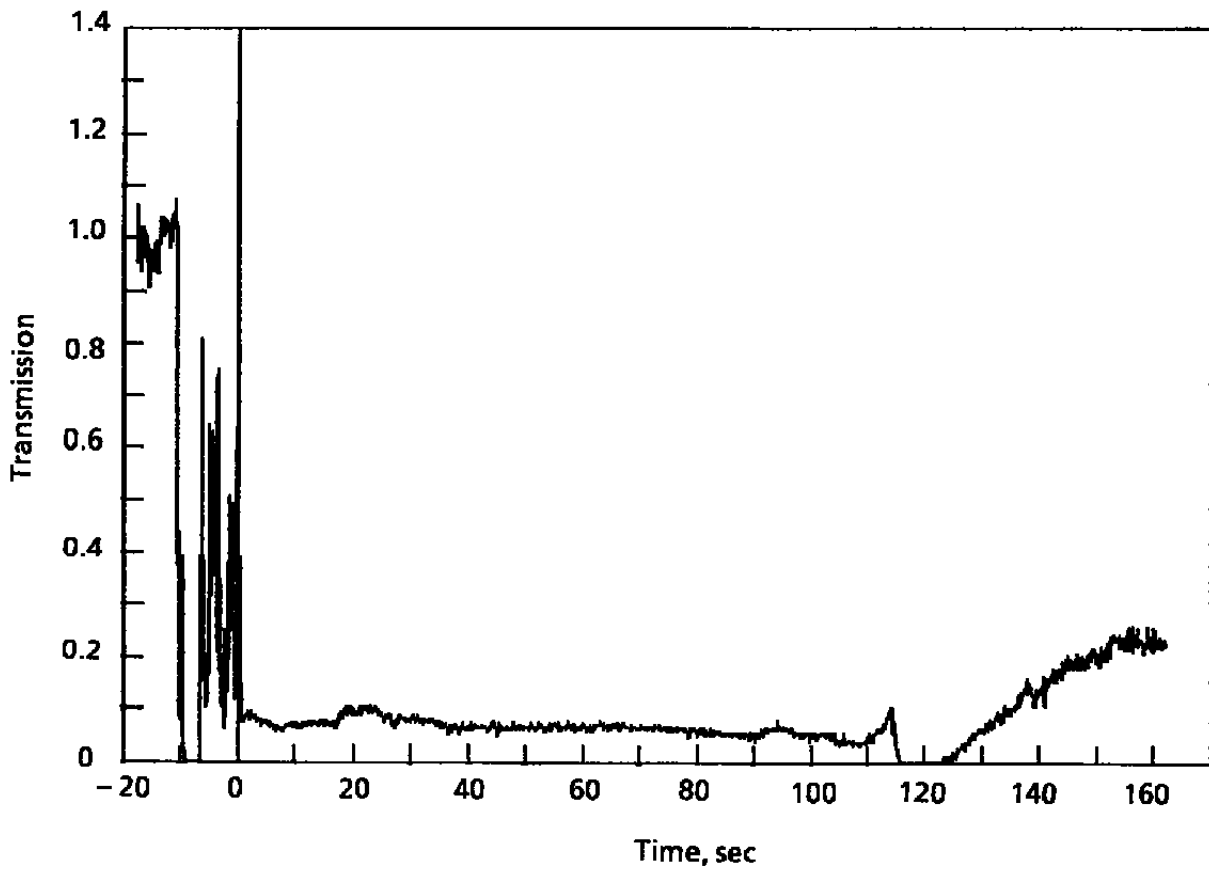
Side View

Transmitters

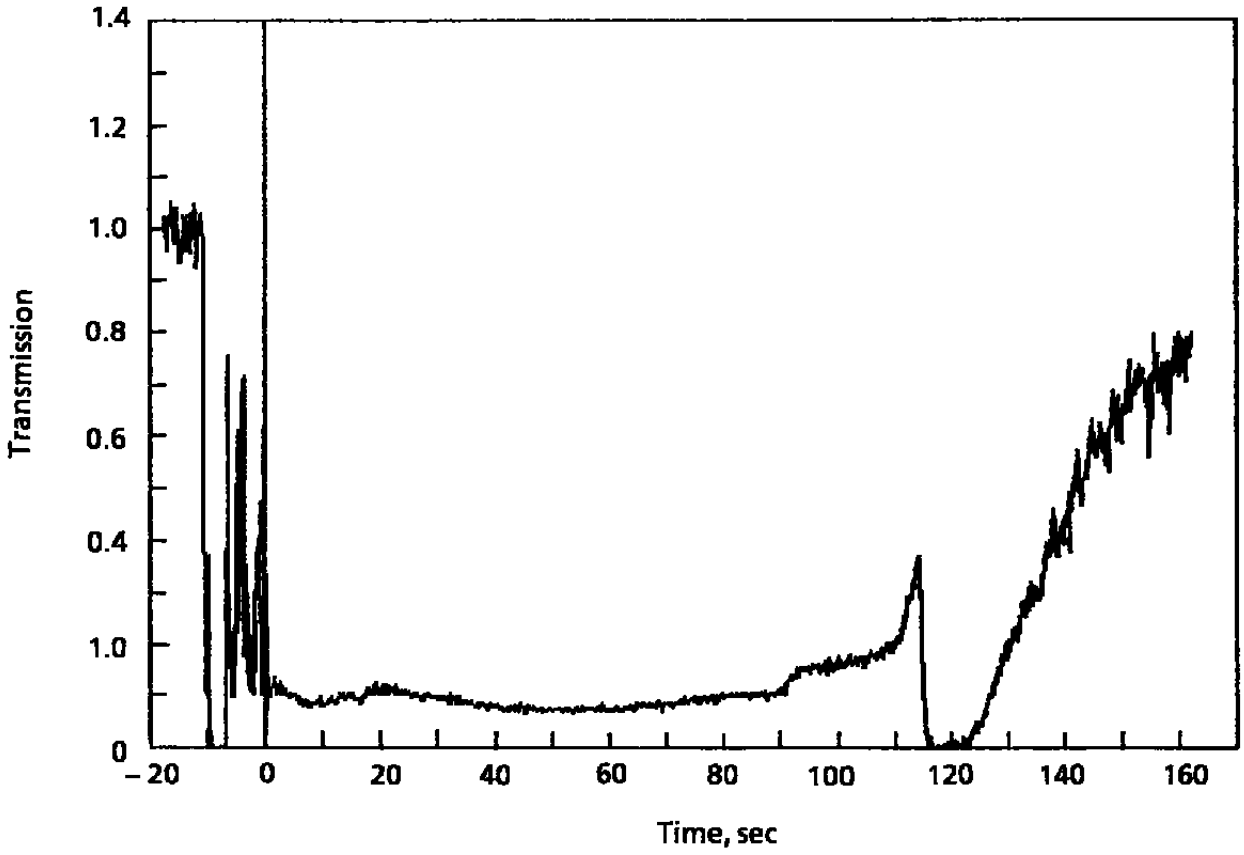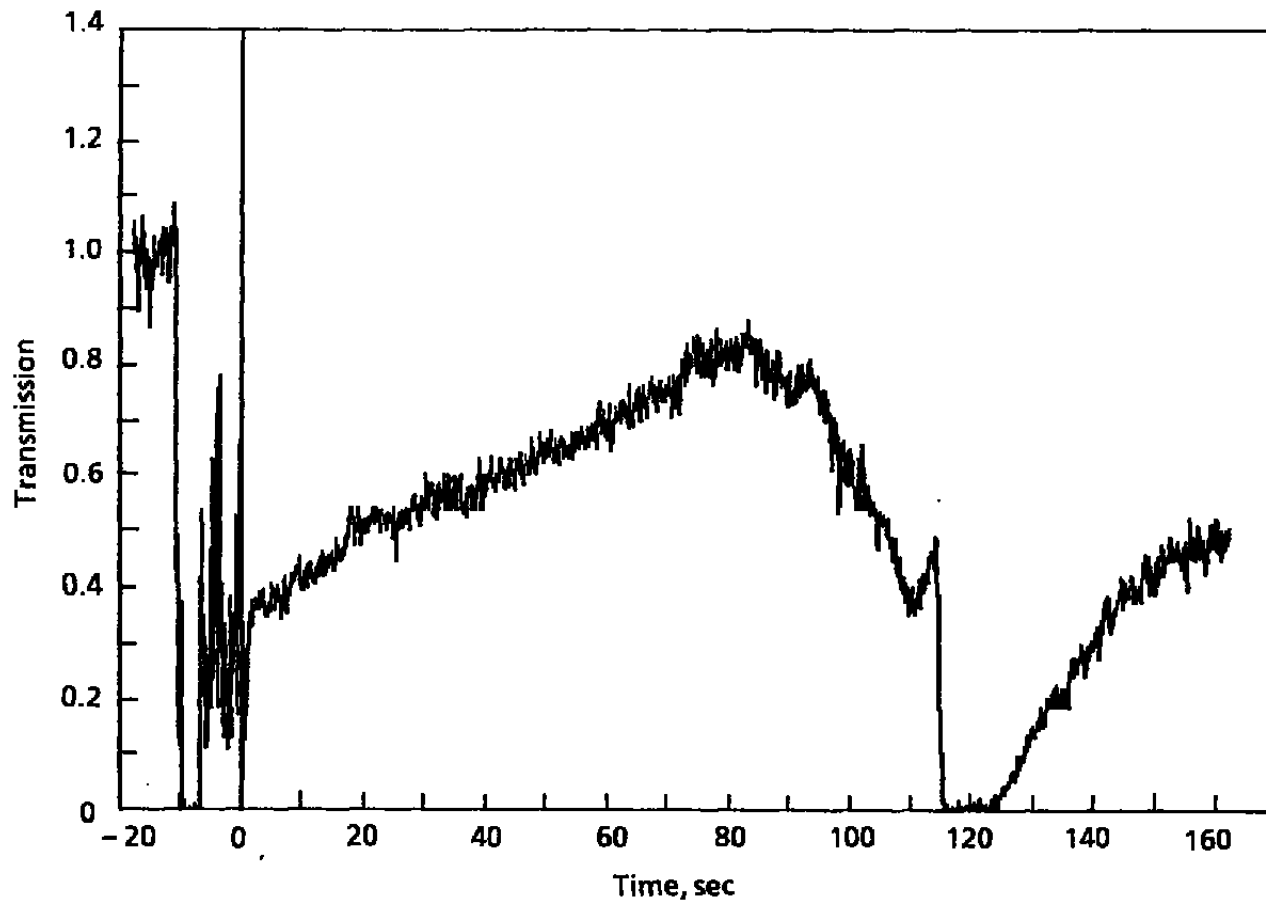Figure 16. Nd:YAG laser system.

a. Path 1, r = 2.5 in.
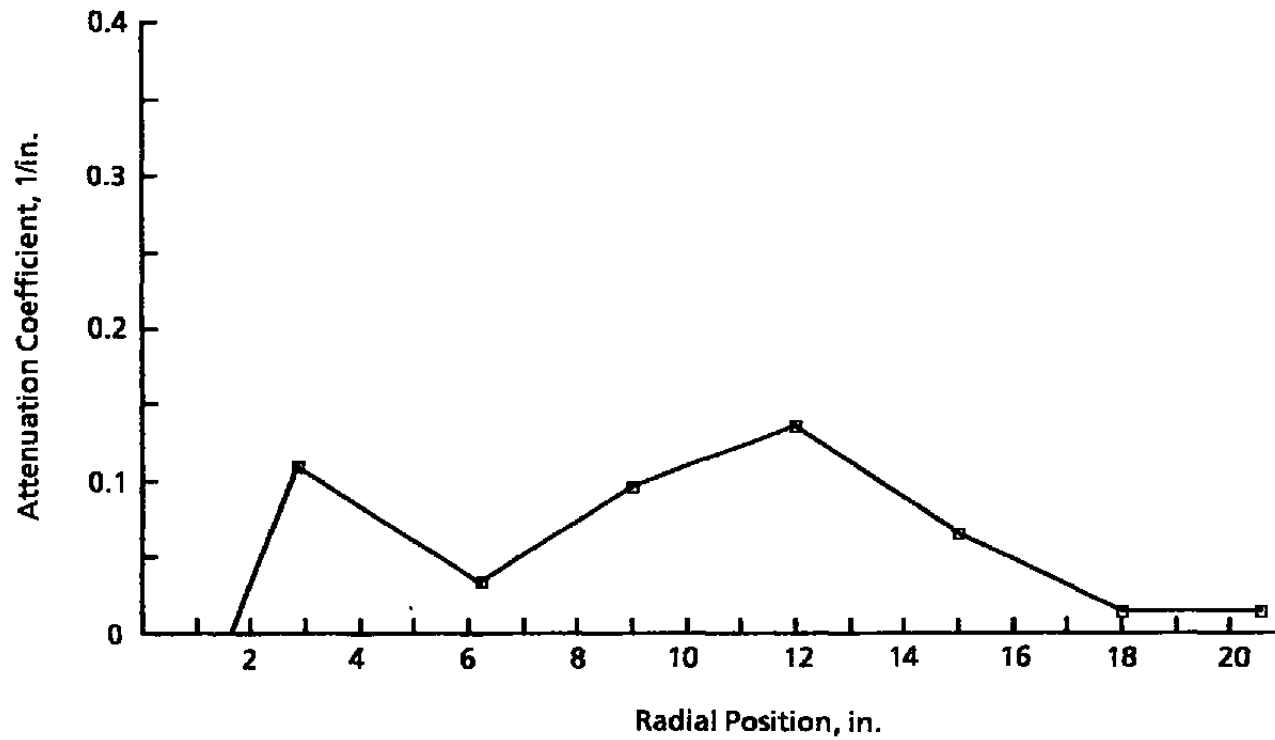Figure 17. 1.06-μm laser transmission (I/I$_0$) versus time, nonspin motor.

b. Path 3, r = 8.1 in.
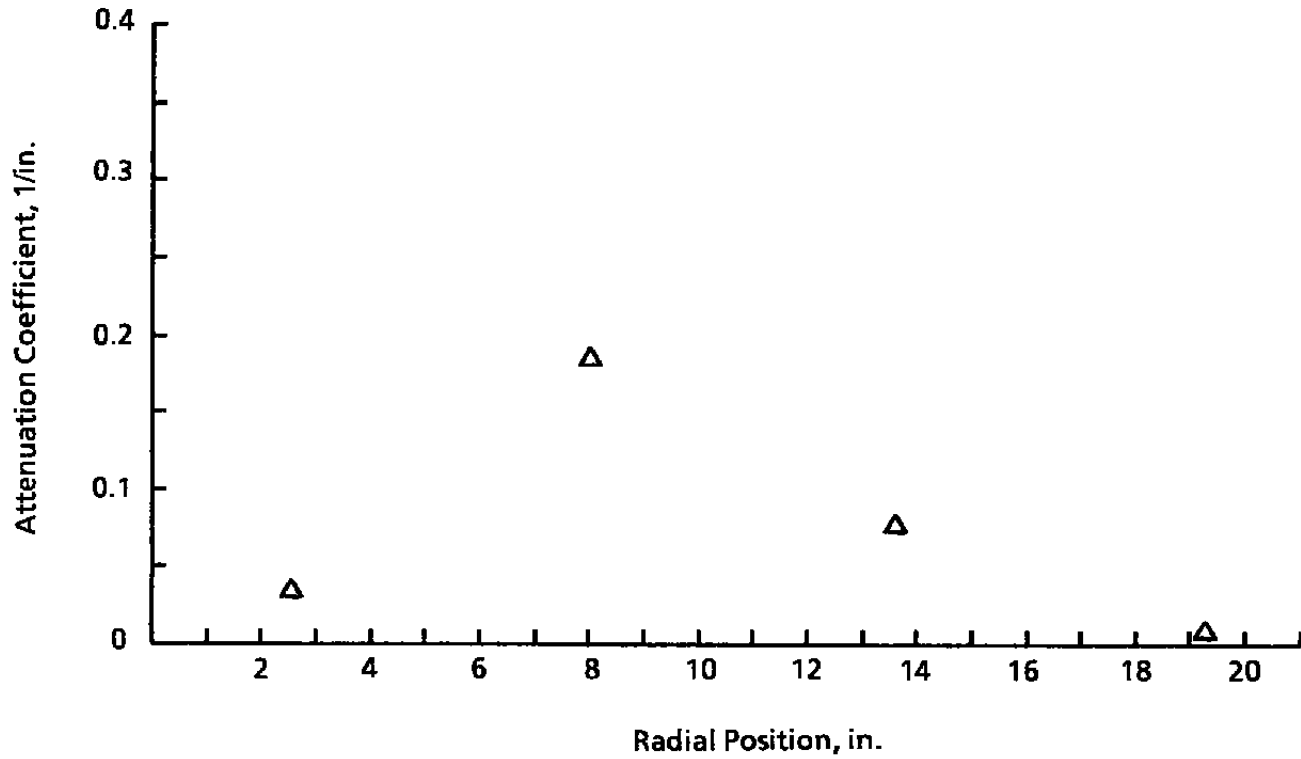Figure 17. Continued.

c. Path 5, r = 13.7 in.
Figure 17. Continued.

d. Path 7, r = 19.1 in.
Figure 17. Concluded.

Figure 18. Attenuation coefficient radial profile, nonspin motor.

Figure 19. Attenuation coefficient radial profile, spin motor.

Table 1. AEDC Plume Instrumentation

Instrument	Spectral Range, μm	FOV Axial Distance from Nozzle Exit, in.	FOV Radial Distance from Nozzle Centerline, in.	FOV
Nd:YAG Laser	1.06	5.5 (T-1); 11.0 (T-2)	0,3,6,9,12,15,18,21	1.0 in.
Nd:YAG Laser (Spin Test Only)	0.53	5.5	0,3,6,9,12,15,18,21	1.0 in.
MEDTHERM® Radiometer No. 1	Total	70 (T-1); 17 (T-2)	0	2 deg
MEDTHERM® Radiometer No. 2	Total	10 (T-1); 29 (T-2)	0	2 deg
MEDTHERM® Radiometer No. 3	Total	4 (T-1); 70 (T-2)	0	2 deg
MEDTHERM® Radiometer No. 4	Total	44 (T-1); 2 (T-2)	0	2 deg
LWIR CVF Spectrometer	2.5 to 14	5 (T-1); 19 (T-2)	0	0.44 deg
UV Spectrometer	0.246 to 0.278	2 (T-1); 17 (T-2)	0 (T-1) 3.0,7.75,12.5,17.25,22.0 (T-2)	6 × 0 in.
Xyboin® Gated Camera Nos. 1, 2	0.4 to 0.9	—	—	Full Plume
SWIR Camera	2.08 to 2.67	—	—	Full Plume
MWIR Camera	4.18 to 4.49	—	—	Full Plume
LWIR Camera	9.0 to 11.5	—	—	Full Plume

Table 2. Summary of Motor Performance

General Information	Spin Test	Nonspin Test
Prefire Motor Case Temperature, °F	35	95
Average Spin Rate, rpm	35.0	N/A
Total Expended Weight (AEDC), lbm	9482.9	9457.5
Prefire Nozzle Exit Area (AEDC), in.^{2}	1217.12	1219.57
Prefire Nozzle Throat Area (AEDC), in.^{2}	15.386	15.555
Nozzle Expansion Ratio	79.1:1	78.4:1
Postfire Nozzle Exit Area (AEDC), in.^{2}	1217.097	1223.474
Postfire Nozzle Throat Area (AEDC), in.^{2}	N/A	21.818

Test Cell Performance

	Spin Test	Nonspin Test
Altitude		
At Motor Ignition, ft	98,000	93,000
Average, ft	113,000	112,000
Pressure		
At Motor Ignition, psia	0.174	0.215
Average, psia	0.088	0.092

Ballistic Performance

	Spin Test	Nonspin Test
Motor Action Time, Sec (Time to 10 psia Motor Chamber Pressure)	117.357	117.008
Motor Ignition Time, msec (Time to 200 psia Motor Chamber Pressure)	250	281
Maximum Motor Chamber Pressure, psia	875.5	902.3
Average Motor Chamber Pressure Over Action Time, psia	706.0	688.0
Maximum Vacuum Thrust, lbf	28,860	29,091
Average Vacuum Thrust Over Action Time, lbf	23,988	24,072
Delivered Specific Impulse Over Action Time, lbf-sec/lbm	299.43	298.70
Effective Specific Impulse Over Action Time, lbf-sec/lbm	296.87	297.81

Table 3. Aluminum Chloride Band Heads

λ	I	V,V	λ	I	V,V	
2708.9 R	2	R 7,9	262.5 R	5	Q 3,3	
2702.3 R	3	R 6,8	2622.4 R	4	R 3,3	
2696.4 R	3	R 5,7	2620.0 R	4	Q 2,2	
2692.8 R	5	Q 4,6	2618.2 R	3	R 2,2	
2685.7 V	6	Q 2,4	2617.0 R	4	Q 1,1	
2683.1 V	6	Q 1,3	2614.4 R	8	Q 0,0	R 1,1
2681.1 V	4	Q 0,2	2610.2 R	6	R 0,0	
2649.7 V	4	Q 1,2	2606.7 R	2	R 6,5	
2647.5 V	6	Q 0,1	2600.7 R	3	R 5,4	
2644.9 R	2	R 7,7	2595.4 R	2	R 4,3	
2638.1 R	3	R 6,6	2590.8 R	2	R 3,2	
2632.8 R	3	Q 5,5	2586.7 R	2	R 2,1	
2632.2 R	3	R 5,5	2564.3 R	1	R 4,2	
2627.8 R	4	Q 4,4	2559.6 R	1	R 3,1	
2627.0 R	3	R 4,4	2555.5 R	1	R 2,0	

Note: The Letters R and V After the Wavelength Indicate the Direction of Degradation of the Band, Whereas the Nature of the Head (R and Q) is Indicated Before the Vibrational Quantum Numbers.

Ref.: *The Identification of Molecular Spectra*, R. W. B. Pearse and A. G. Gayden, Chapman and Hall Ltd., 1950, p. 47.